Hygrothermal assessment of diffusion open insulation systems for interior retrofitting of solid masonry walls

Jensen, N.F.; Odgaard, T.R.; Bjarløv, S.P.; Andersen, B.; Rode, C.; Møller, E.B.

Published in:
Building and Environment

Link to article, DOI:
10.1016/j.buildenv.2020.107011

Publication date:
2020

Document Version
Peer reviewed version

Hygrothermal assessment of diffusion open insulation systems for interior retrofitting of solid masonry walls

N.F. Jensen[a,*], T.R. Odgaard[b], S.P. Bjarløv[a], B. Andersen[c], C. Rode[a], E.B. Møller[a],

[a]Department of Civil Engineering, Technical University of Denmark, Brovej 118, 2800 Kgs. Lyngby, Denmark

[b]COWI A/S, Section of Building Physics and Refurbishment, Parallelvej 2, 2800 Kgs. Lyngby, Denmark

[c]Department of Bioengineering, Technical University of Denmark, Søltofts Plads Building 221, 2800 Kgs. Lyngby, Denmark

Highlights:

- Hygrothermal assessment of three diffusion-open capillary active insulation systems
- Investigation of the effect of exterior hydrophobisation of solid masonry
- Poor hygrothermal performance was seen for all systems without hydrophobisation
- Good performance for PUR foam with calcium silicate channel when hydrophobised
- High pH of adhesive mortars seems to prevent mould growth behind the insulation

Keywords: interior insulation, solid masonry, field study, hydrophobisation, mould modelling, on-site mould observations

Abstract

The present project investigated the hygrothermal performance and risk of mould growth in solid masonry walls fitted with three diffusion-open capillary active interior insulation systems installed in

* *Corresponding author.
E-mail addresses: nicf@byg.dtu.dk (N.F. Jensen).

containers with a controlled indoor climate. The project was carried out as a large experimental study in two 40-feet reefer containers reconfigured with 24 holes (1x2 m), in which solid masonry walls with embedded wooden elements were installed. The focus of the study was on the conditions in the interface between the masonry and the interior insulation, and in the embedded wooden elements. The effect of exterior hydrophobisation was also investigated. Relative humidity and temperature were measured at several locations in the test walls over a period of four years. The findings indicate that exposed walls with interior insulation and high indoor RH performed poorly in terms of the risk of mould growth. Combined with exterior hydrophobisation against driving rain, the semi diffusion-tight insulation system performed better than the highly diffusion-open systems. Good performance was observed for the semi diffusion-tight polyurethane foam insulation with calcium silicate channels combined with exterior hydrophobisation. The effect of hydrophobisation varied with the orientation. Mould observations found no growth in the interface in most walls, probably because the high alkalinity of the adhesive mortars and scarce nutrition prevented growth. Growth was however found in some walls having low alkalinity and possibly available nutrition. Little correlation was found between on-site and modelled mould growth.

1 Introduction

Studies of the Danish building stock have shown great potential for energy conservation by retrofitting external walls, especially solid masonry walls, in buildings constructed prior to 1930 [1]–[5]. Solid masonry buildings constructed in the period 1850-1930 account for 41% of all Danish multi-story residential buildings (3-6+ floors), and 25% of all apartments [5]. National data from the EU Energy Performance Certificates database indicate an average-weighted U-value of 0.83 and 1.12 $W/m^2 \cdot K$ for

external walls in multi-story residential buildings built prior to 1850 and in the period 1850-1930, respectively [4]. The external appearance of many of the aforementioned buildings is worthy of preservation, placing several constraints on exterior alterations. Sizable energy savings were found in previous theoretical [5]–[8] and field studies [9]–[16] of internally insulated solid masonry walls.

Internally retrofitted insulation is considered risky as it alters the thermal and moisture balance of the existing wall structure. The reduced heat flow alters the temperature gradient in the existing wall as the external wall becomes colder [13], [17]–[21], increasing the risk of interstitial condensation between the existing wall and the new insulation [17], [18], [22]–[24]. Moreover, the increased diffusion resistance of the new insulation reduces the inward moisture diffusion that contributes to drying the masonry wall [14], [18]. The higher moisture levels lead to increased risk of moisture-induced damage, including frost damage [18], [19], [23]–[25], mould growth [6], [17], [18], [22], [26], [27], and wood decay [18], [25], [27]. Despite these disadvantages, internal insulation may sometimes be the only retrofit option that preserves cultural heritage, such as the architectural significance. Mineral wool and vapour barriers have traditionally been used for internal retrofitting [17], [21], [22], [26]. In many cases, this traditional method has resulted in mould growth caused by solar-driven vapour flow from the outside towards the inside during periods with alternating rain and solar exposure [26], [28]. Other potential problems include mechanical damage to the vapour barrier or poor craftsmanship, either of which can allow moist indoor air to diffuse outwards into the masonry [26].

In recent years, internal insulation strategies have changed focus from diffusion-tight systems towards diffusion-open capillary active systems allowing redistribution of moisture, in order to reduce the mould risk. In [29], [30] the effects of the material properties of insulation and adhesive on moisture redistribution were investigated. The findings suggest that improved performance could be obtained by using insulation with higher water conductivity. Studies [6], [9], [10], [14], [16], [31]–[35] observed that good performance could be obtained by using diffusion-open capillary systems for internal retrofitting. In some of the studies the good performance that was observed could have been due

either to exterior rain protection or a low internal moisture load. Other studies [36]–[39] have found high relative humidity (RH) levels in the interface when diffusion-open capillary systems had been used. In [25], [39]–[43], diffusion-open and diffusion-tight systems were compared: lower RH levels were observed in the interface in [41], and in [42], [43] lower RH was observed in beam ends for the diffusion-tight systems. Note that in these studies driving rain was excluded or limited by fitting exterior protection. Vereecken and Roels [40] observed better performance for diffusion-tight systems under quasi steady-state winter conditions (without rain), and Vereecken et al. [25] concluded from hygrothermal simulations that if rain could be disregarded then there was no reason to use diffusion-open capillary systems.

Wind Driven Rain (WDR) is one of the largest sources of moisture in the walls of buildings [18]. Studies [7], [13], [39], [44]–[46] found WDR to be one of the crucial factors that determine the performance of internally insulated solid exterior walls. Exterior rain protection such as hydrophobisation is often proposed for buildings worth preserving [23], [36]. In [47]–[50] excellent water-repellent performance was observed for various brick types using different hydrophobisation agents. In [49] a less pronounced effect was observed for mortar samples. A key feature of the hydrophobisation is not to alter the vapour diffusion resistance of the building [51]. In [49] no significant increase was documented for the vapour diffusion resistance. Reduced evaporative drying potential was however observed in [50]. Some studies [6], [8], [52], [53] found improved hygrothermal performance using exterior hydrophobisation, while increased RH levels were found for exterior protection that used render and paint [41]. However, other studies using exterior render and paint [10], [34], [35] found good performance in the interface (possibly due instead to a low internal moisture load). Although hydrophobisation appears to be an excellent solution, [26] listed several limitations that must be considered, including problems with overall tightness and surface defects . Studies [12], [33], [39], [46], [52] have found that orientation was of great importance for the efficacy of internal insulation. High solar exposure on walls will contribute significant drying [18] but may also cause inward solar-driven vapour flow.

Several studies have found unacceptable moisture levels resulting from internal insulation retrofits, but as common indoor mould species typically thrive at pH-values 4-9 [54] and manufacturers claim [55]–[57] that the high alkalinity of the glue mortars used in the installation of insulation products prevents mould growth, there has been a focus on the alkalinity of the glue mortars. Morelli and Møller [16] found a high pH-value (using phenolphthalein) and no mould growth behind the internal insulation after two years.

The purpose of this study was to assess the hygrothermal performance of three diffusion-open capillary systems. One aim was to determine if exterior hydrophobisation improved the hygrothermal performance of diffusion-open capillary active systems by preventing the absorption of WDR. Another aim was to test whether theoretical mould models would be useful for the prediction of mould risk in the interface and in embedded wood elements, in solid masonry retrofitted with internal insulation, by comparing their predictions with on-site Mycometer testing.

2 Methods

A large experimental setup was constructed at the Department of Civil Engineering of the Technical University of Denmark (DTU) on a test site in Kongens Lyngby, Denmark (55.79°N, 12.53°E). The experimental setup comprised several test walls constructed to emulate a section of a Danish historic multi-story building from the period 1850-1930, both in relation to design and materials. The setup was designed to investigate the application of several diffusion-open capillary active interior insulation systems applied to solid masonry walls with embedded wooden elements.

2.1 Test stand

The experimental setup comprised two insulated reefer containers with the external dimensions (LxWxH): 12.2 m by 2.4 m by 2.9 m, with an interior volume of 67.6 m^3. The containers were

abbreviated “G” and “X”. Twenty-four 1 x 2 m cut-outs were made in the façades to accommodate the test walls. The holes were spaced 0.4 m apart. Next, twenty-four identical test walls with the dimensions (HxWxD) 1987 mm by 948 mm by 358 mm (1½ stones thick with 10 mm interior rendering) were constructed in façade cut-outs (Figure 1 and 2). Each represents a different design scenario. To simulate problems with thermal bridges at the joints with adjacent elements, the test walls were constructed as a 3-dimensional set-up including a wooden floor construction and a 108 mm (½-stone) interior masonry wall with render on both sides. The wooden floor construction consisted of a 175 x 175 mm wooden beam end embedded 100 mm into the masonry wall, supported by a 100 x 100 mm embedded wooden wall plate. The wooden elements were made from ordinary construction timber (Pomeranian pine wood). The floor construction was closed off using 15 mm thick Oriented Strand Board (OSB), and 100 mm of mineral wool was used to emulate the clay-pugging layer traditionally placed between floor beams. To best emulate the hygrothermal conditions occurring in Danish historic buildings between 1850 and 1930, the test walls were constructed using yellow soft-moulded masonry bricks and 7.7% lime adjusted mortar (air lime), grain size 0-4 mm. The same lime mortar was used also as interior render.

The masonry walls were constructed from early August to mid-September 2014 and allowed to dry for 5-6 months until the installation of the insulation systems in mid-February and March 2015. Furthermore, from early December 2014 until mid-April 2015 forced drying was performed by heating the indoor climate to 40–50 °C, resulting in an indoor RH of 10–30%.

The experimental setup was constructed with special care and attention directed towards the reduction of potential sources of error from unintentional heat, air or moisture transport. The measures taken were:

- Hygric and thermal decoupling: To control heat, air and moisture transport, 400 mm mineral wool (λ = 0.037 W/(m·K)) was installed between the test apertures and 150 mm above them,

and a vapour barrier was located between the test walls and the container walls, floor and ceiling.

- Sealing of joints: Mastic sealant was used to seal off joints between test walls and container walls, to prevent rain intrusion.
- Rainwater run-off: A roof with rain gutters was constructed on top of the containers, and flashings were installed directly above each test wall to prevent rain entering the walls through the horizontal sections sticking out through the container walls, as illustrated in Figure 1a.
- Preventing rain splash-up: The containers were raised ≥ 350 mm off the ground.

No thermal decoupling was carried out between the container floor and test walls besides the thermal resistance of the container floor itself. The lack of thermal decoupling for the floor was however not considered an issue, as the nearest sensor was located approximately 800 mm above floor level.

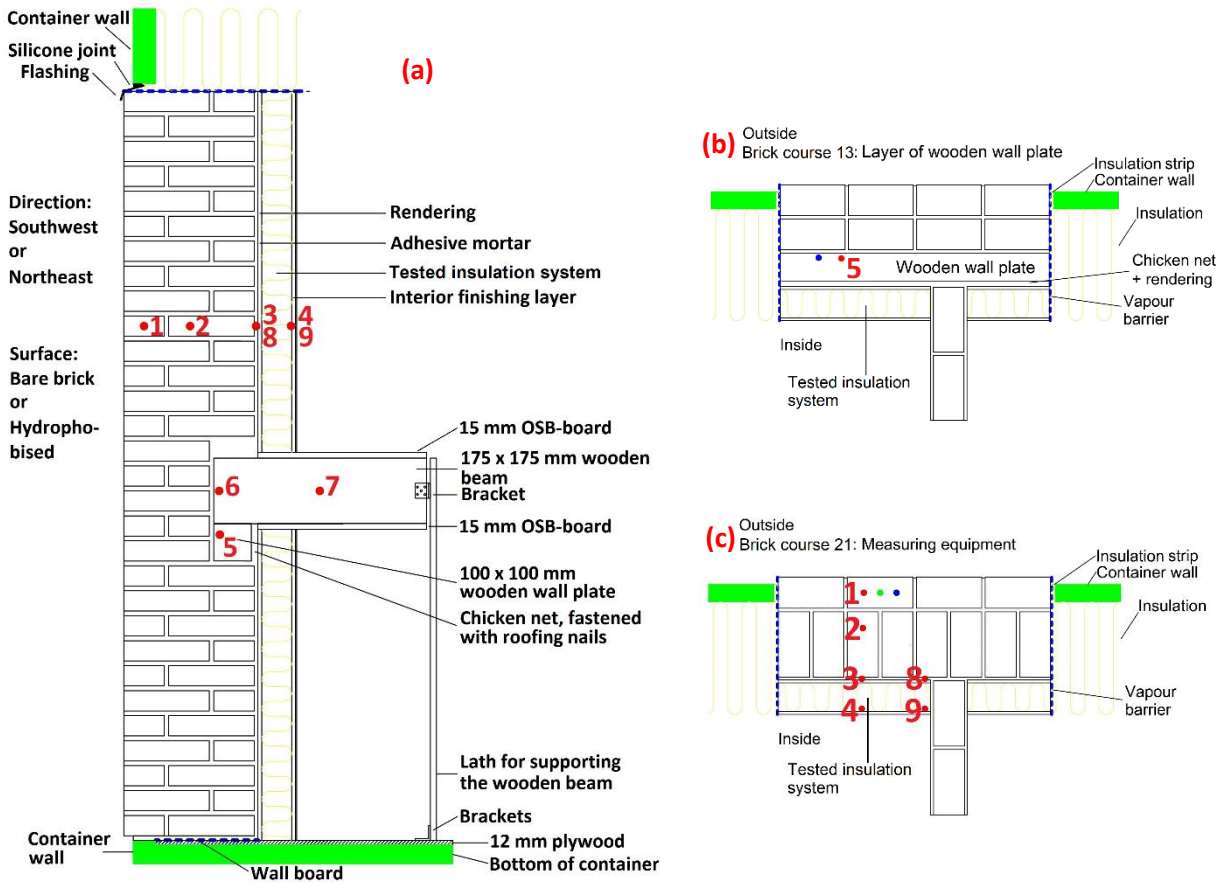

Figure 1 Test stand configuration: (a): Vertical section of a test wall, (b): Horizontal section through the 13th brick course, (c): Horizontal section through the 21st brick course. Source: Tommy Riviere Odgaard.

Figure 2 The experimental setup: (a): The test containers, (b): installation of the embedded wooden wall plate, (c): installation of sensors in the masonry bricks, (d): installation of the embedded wooden beam end, (e): the internal insulation with embedded sensors, (f): external treatment with hydrophobising cream. Source: Tommy Riviere Odgaard.

2.1.1 Wall insulation configurations

Results from twelve of the twenty-four test walls are presented in this paper, and the wall configurations are presented in Table 1. Four insulation systems were assessed in a temperate Nordic climate: 1) composite material of polyurethane foam with calcium silicate channels in a grid of 40 mm by 40 mm (PUR-CM), 2) calcium silicate (CaSi), 3) lightweight autoclaved aerated concrete (AAC) , and 4) a traditional system of mineral wool and vapour barrier (MW). Insulation systems were applied to the base walls, while three base walls were left as uninsulated reference walls: G3 (SW), G14 (NE) and X5 (SW). Test walls were kept as bare brick on the exterior surfaces, except for G2, G15, and X3. These walls were treated with a silane/siloxane-based hydrophobising cream with 40% active ingredient. The interior surfaces were treated with diffusion-open paint, except for G1 which was treated with traditional diffusion-tight paint. Each insulation systems was installed by specially trained workers

174 from the respective companies and the exterior hydrophobisation was applied according to the
175 manufacturer's recommendations. As shown in Table 1, the systems with MW and PUR-CM are
176 considerably more vapour tight than the systems with CaSi and AAC.

177

178 **2.1.2 Measurement equipment**

179 Throughout the experiment, temperature and RH were measured and logged every 10 minutes using
180 digital HYT221 sensors from Innovative Sensor Technology IST AG [58]. Sensors were installed and
181 embedded in nine different locations in each test wall (Figure 1 red dots), two in each container for
182 the indoor climate and three for the outdoor climate. Prior to installation the HYT sensors were sealed
183 with shrink-rubber with the exception of the sensing area, and drilling holes were sealed with silicone
184 sealant and a small blocking plate to prevent the silicone from covering the sensor head. Sensor
185 accuracy was 0.2 K between 0 and 60 °C for temperature, and 1.8% at 23 °C between 0 and 90% for
186 RH. Sensor range was -40 to 125 °C and 1 to 100% RH. Sensors were calibrated using saturated salt
187 solutions prior to installation. The rate of missing sensor data was quite low, and due to loggings every
188 10 minutes the date are considered as secure. Over the course of the experiment two periods of +10
189 days occurred without measurements due to system malfunctions, these periods are visible in the
190 figures.

191

192 Table 1 Wall configurations and properties used in the field study. The insulation systems were applied internally
193 to the base wall configuration. The three reference walls G3, G14, and X5 were kept as uninsulated base walls.

No. of walls: Wall ID & orientation	Material layers (exterior side on top and interior side in the bottom)	Density [kg/m³]	λ_{dry} [W/(m·K)]	μ_{dry} [-]	A_w [kg/(m²·s^{½})]	d [mm]	R [m2·K/W]	Z [m²·s·Pa/kg]
Base walls	Yellow masonry brick*	1643	0.600	16.9	0.278	348	0.58	2.97E+10
	7.7% lime mortar*	1243	0.440	22.43	0.390	10	0.02	1.13E+09
	Total: existing wall						**0.60**	**3.08E+10**
1 wall: G1_MW_SW	Mineral wool	37	0.040	1	0	100	2.50	5.05E+08
	Vapour barrier			700000		0.2		7.07E+11

	Gypsum board	850	0.200	10	0.277	13	0.07	6.57E+08
	Paint							1.73E+09
	Total: MW system						**2.57**	**7.10E+11**
4 walls: G2_PUR-CM+H_SW G7_PUR-CM _SW G10_PUR-CM _NE G15_PUR-CM+H_NE	PUR-CM adhesive mortar	1313	0.497	18.75	0.005	10	0.02	9.47E+08
	PUR-CM insulation	49	0.037	27.01	0.013	80	2.16	1.09E+10
	PUR-CM render	725	0.147	11.73	0.107	10	0.07	5.92E+08
	PUR-CM surface filler	1270	0.479	14	0.222	3	0.01	2.12E+08
	Paint							5.26E+07
	Total: PUR-CM system						**2.26**	**1.27E+10**
2 walls: G4_CaSi_SW G13_CaSi_NE	CaSi adhesive mortar*	1655	0.500	6.60	0.600	10	0.02	3.33E+08
	CaSi insulation*	225	0.061	4.23	0.726	100	1.64	2.14E+09
	CaSi adhesive mortar*	1655	0.500	6.60	0.600	8	0.02	2.67E+08
	Paint							1.58E+08
	Total: CaSi system						**1.68**	**2.90E+09**
2 walls: X2_AAC_SW X3_AAC+H_SW	AAC adhesive mortar*	830	0.155	13	0.003	8	0.05	5.25E+08
	AAC insulation board*	99	0.044	3	0.006	100	2.27	1.52E+09
	AAC adhesive mortar*	830	0.155	13	0.003	8	0.05	5.25E+08
	Paint							1.32E+08
	Total: AAC system						**2.38**	**2.70E+09**

*materials tested by Technische Universität Dresden, unmarked parameters were from the Delphin [59] material database or manufacturer data. G: container 1, X: container 2, SW: south-west, NE: north-east, +H: exterior hydrophobisation.

2.1.3 Boundary conditions

The indoor boundary conditions were kept at 20 °C and 70% RH during the initial period (May to August 2015), to stress the experiment. Afterwards the setpoint was reduced to 20 °C and 60% RH, equal to a water vapour content of 10 g/m^3, which corresponds to the highest humidity class for dwellings (humidity class 3) in the Danish context [17]. The containers were conditioned using humidifiers and heating fans. However, no cooling or dehumidification was installed, so fluctuations due to high temperature or humidity could occur. Furthermore, the containers were fitted with two fresh air fans, providing an air change rate of approximately 0.5 h^{-1}, the minimum rate permitted by Danish building regulations [60].

In Denmark, south-west is the prevailing wind direction and thus the most critical in terms of WDR. A combination of WDR with high solar irradiation on a south-facing wall may lead to moisture transport

209 towards the indoor environment. A north-facing wall receives less WDR, but at the same time less
210 solar irradiation. To assess both of these scenarios, eight of the twelve test walls faced south-west
211 (237°), and four faced north-east (57°) (Table 1). The test containers were installed so WDR would not
212 be obstructed by nearby buildings, and so shadows onto to the wall surfaces were minimal.

213

214 **2.2 Mould growth**

215 **2.2.1 On-site mould testing**

216 Mould growth was measured on-site using Mycometer Surface and Bulk-material tests (quantitative)
217 [61], and swab tests to determine mould species (qualitative). Surface tests were used to determine
218 growth in the interface between the existing wall and the insulation system, while the bulk-material
219 test was used to assess growth in the different layers of the insulation system.

220 Samples were taken using a 100 mm hole-saw (without a pilot bit). The core sample was immediately
221 placed in a sealed container, after which Mycometer surface and swab samples were taken in the
222 interface thus exposed (two of each). In the laboratory, the outer material of the core sample was cut
223 away leaving a 20 mm by 20 mm central core (Figure 3c). The central core was divided into three
224 sections for the bulk-material test: 1) outermost 10 mm (nearest to the interface), 2) middle section
225 11-55 mm, and 3) innermost section 56-100 mm (near the interior surface). The bulk-material test was
226 only performed for the middle or innermost sections if growth was detected in the outermost section
227 of the central core.

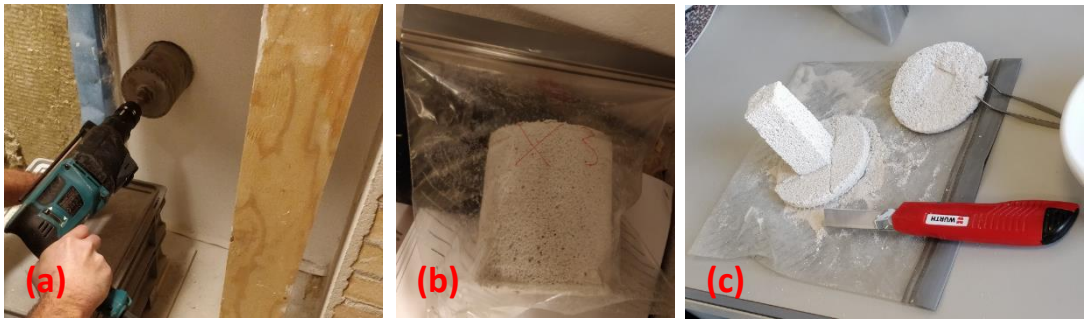

Figure 3 Mould sampling: (a): the hole-saw, (b): sealed core sample, and (c): preparation of Mycometer bulk-material samples. Source: Nickolaj Feldt Jensen

Mould samples were taken in November 2018, 3½ years after commencing the experiment. Additional samples were taken for walls X2-X3 in March 2019, and another full set in September 2019.

Swab tests were streaked out on V8 and DG18 media, then incubated at 20 °C in darkness for 7 days. Fungal colonies were transferred to CYA, MEA and YES media, and incubated at 25 °C in darkness for 7 days and identified under stereo and light microscopes [62]. The Mycometer test measures the fluorescent product released from the enzyme-substrate complex relating to the N-acetylhexosaminidase activity found in mould growth to determine the extent of the growth [61]. Mycometer surface tests were performed according to [63]–[65] and the bulk-material tests were performed according to [66], [67]. The Mycometer values (MV) obtained were evaluated as:

- Category A (green), normal background level: MV ≤ 25 (surface) or MV ≤ 150 (Bulk-material)
- Category B (yellow), above normal background level: 25 < MV < 450 (surface) or 150 < MV < 450 (Bulk-material)
- Category C (red), a high level of fungi: MV > 450

The accuracy of the Mycometer method was evaluated by the US EPA [68] who found that the standard deviation between tests was around 5-10% for tests with fungal spores from *Aspergillus flavus* and *Cladosporium herbarum*.

2.2.2 Mathematical mould-growth models

Three widely used mould-growth models were applied for post processing of measurements to assess the hygrothermal conditions of the test walls over time and produce a theoretical prediction of the risk of mould growth.

The VTT model: by Hukka and Viitanen [69]. The output of this model is the mould index (*M*), ranging from 0 to 6, where 0 corresponds no growth and 6 to heavy growth (100% coverage). Values 3-6 are within the visual range. Interface (point 3) was assumed to be "medium resistant" with a decline factor "relatively low". Embedded wooden wall plates (point 5) and the interface for wall G1 were assumed to be "sensitive" with a decline factor "wood recession".

The MRD model: by Thelandersson and Isaksson [70]. A dose-response model which predicts the limit state "onset of mould growth" defined in the mould rating scale by Johansson [71]. The scale ranges from 0 to 4, where 0 corresponding to no growth, 2 to onset of mould growth and 4 to heavy mould growth. Interface (point 3) was assumed to have a critical dose D_{crit} (material sensitivity) of 102 days (PUR-CM, CaSi and AAC). Embedded wooden wall plates (point 5) and the interface for wall G1 were assumed to have a critical dose D_{crit} of 12 days (planned pine). D_{crit} values were obtained from [72]–[74].

WUFI-Bio [75]: based on the biohygrothermal model of Sedlbauer [76]. This model calculates the moisture balance in mould spores and compares it to what is estimated to be the critical moisture content for spore germination. The model has two outputs: 1) mould growth in mm, and 2) mould index (*M*) according to the VTT model [77]. Interface (point 3) was assumed to be "substrate group II", building materials containing some biodegradable compounds. Embedded wooden wall plate (point 5) and the interface for wall G1 were assumed to be "substrate group I", biodegradable building materials.

Mould predictions for the interface were started after one year (on 01-05-2016) to emulate the effect of the alkaline conditions during the initial dry out process for systems using adhesive mortars

(cementitious materials) as suggested in [78]. Wall G1 was started on 01-05-2015, as no adhesive mortar was used.

In this study the models were compared to Mycometer surface results in the interface.

2.3 pH-value

Samples were taken for the internal lime render and adhesive mortars, to determine their pH-value. Samples were crushed into powder, and 5 g of powder was mixed with 12.5 ml demineralized water. Samples were shaken for 60 minutes at 260-270 rpm, followed by a 10 minute settling period before testing. pH measurement were performed using a Sension+ MM374 (accuracy: ≤0.002 pH) [79]. Two tests were performed for each material sample. The pH value for fresh adhesive mortar powder mixed with demineralized water was similarly determined.

3 Results

Graphical representations of measurement data are based on a 96-hour running average, while plots for mould modelling are shown as hourly values. Supplementary plots and datasets are available in [80]. Plot abbreviations as presented in Section 2.1.1.

3.1 Measurements

3.1.1 Boundary conditions

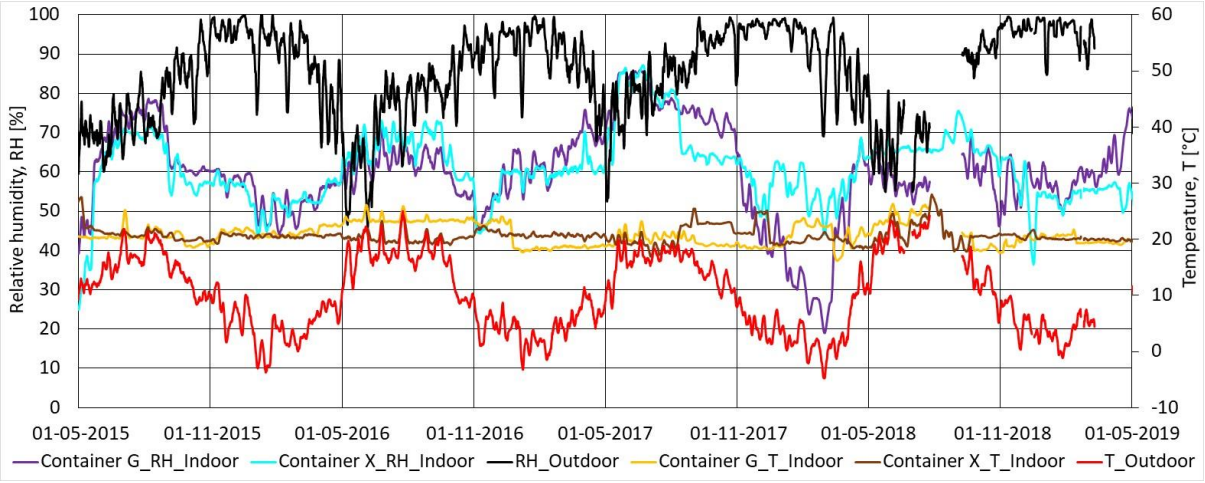

Figure 4 RH and temperature for indoor and outdoor climates

The indoor and outdoor boundary conditions were as shown in Figure 4. The two indoor sensors showed only minor differences between the measured RH and temperatures. The large decrease in the indoor RH levels in container G during the winter of 2018 was caused by a faulty humidifier, which was seen to cause a drop in the RH levels near the interior surface as shown in Figure 5. In terms of WDR load, the measurements showed about three times more rain striking the south-west facing walls in comparison to the north-east facing walls, see [80].

3.1.2 System comparison

This section presents a comparison between the various insulation systems.

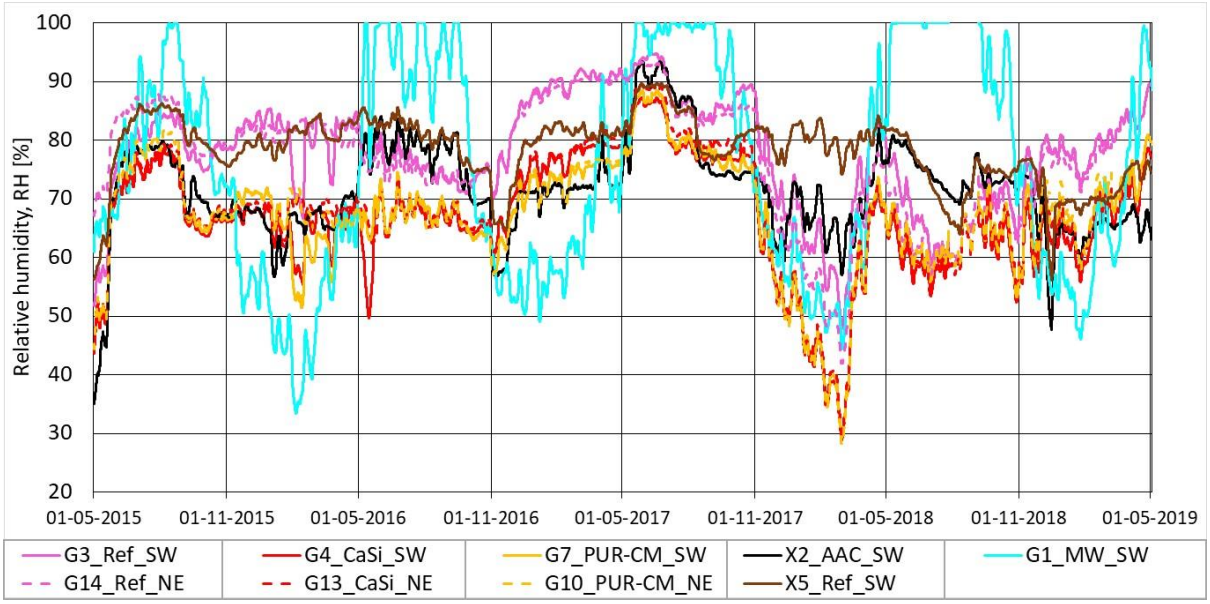

304

305

306 Figure 5 RH in point 4, near interior surface (point 3 for the reference walls G3, G14, and X5)

307 Measurements for the interior surface (Figure 5) showed that RH levels followed the indoor conditions
308 (Figure 4), with a small excess caused by the lower surface temperature, and the moisture content in
309 the test walls, except for the wall with MW. The diffusion-open systems were found to have a lower
310 RH near the interior surface throughout the experiment, compared to the uninsulated reference wall.
311 Minor differences were observed between the different diffusion-open systems. The diffusion-tight
312 MW system was found to have the lowest RH of all systems during winter, and the highest during
313 summer. Only minor differences were observed between orientations.

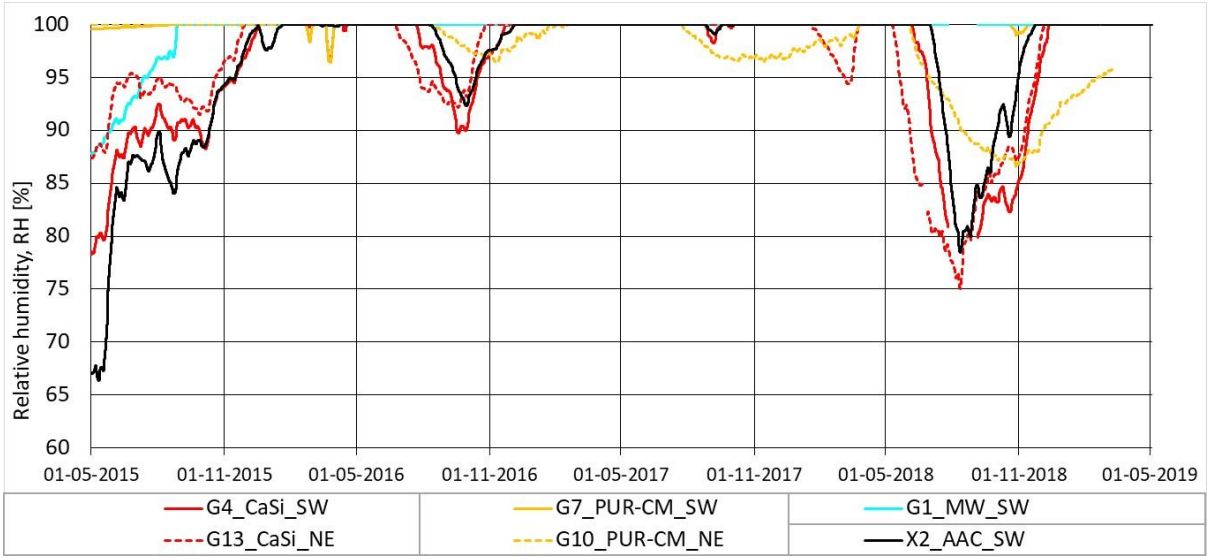

Figure 6 RH in point 3, interface

Measurements in the interface between existing wall and insulation systems (Figure 6) showed that all the test walls experienced unacceptably high RH, with occasional drops during summer and in early autumn. Smaller seasonal fluctuations were observed for the tighter systems (MW and PUR-CM), and only minor differences were observed between the two orientations. The warm dry summer of 2018 greatly reduced RH in the interface for most of the diffusion-open capillary systems.

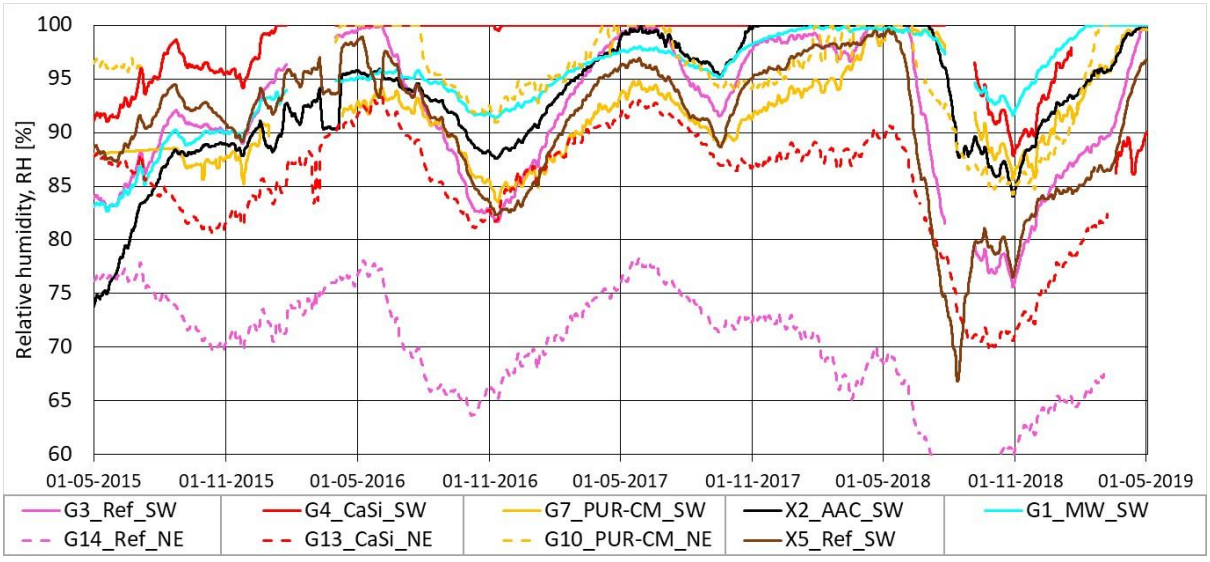

Figure 7 RH in point 5, wall plate

Measurements for the wall plate (Figure 7) showed increasing RH in all the test walls, except the Ref_NE and CaSi_NE walls. Most walls experienced unacceptably high RH, and all of them, except PUR-CM_SW, showed higher RH than their uninsulated reference wall. The CaSi_NE showed considerably lower RH than the CaSi_SW, while smaller differences were observed between the two orientations for the PUR-CM system.

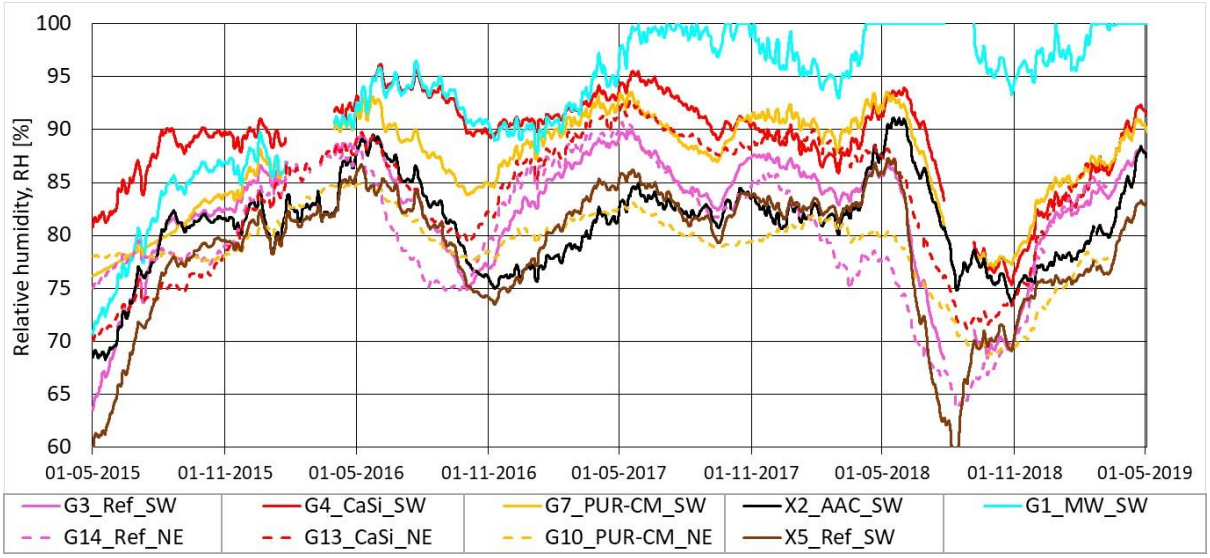

Figure 8 RH in point 6, beam end

Measurements for the beam end (Figure 8) showed lower RH in the diffusion-open capillary systems compared to the diffusion-tight MW system. The MW system showed progressively increasing values, with peaks occurring during the summer periods. All of the test walls, except the PUR-CM_NE and AAC_SW walls, showed higher RH than their uninsulated reference wall. The north-eastern walls were found to have a lower RH than their south-western counterpart.

3.1.3 Effect of exterior hydrophobisation

This section presents the effect of exterior hydrophobisation.

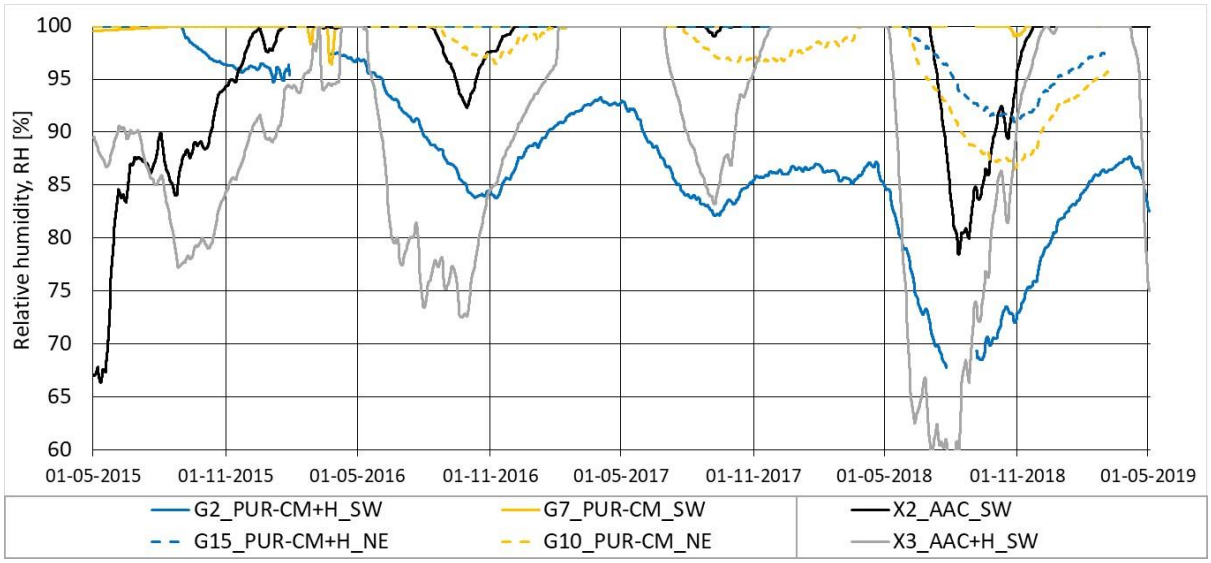

Figure 9 RH in point 3, interface

Measurements for the interface (Figure 9) showed that exterior hydrophobisation generally had a positive effect. The PUR-CM+H_SW wall became progressively drier. The AAC+H_SW did however show rapid drying during summer, followed by a rapid increase in RH during winter. It was observed that the PUR-CM+H_NE performed as poorly as the unhydrophobised wall.

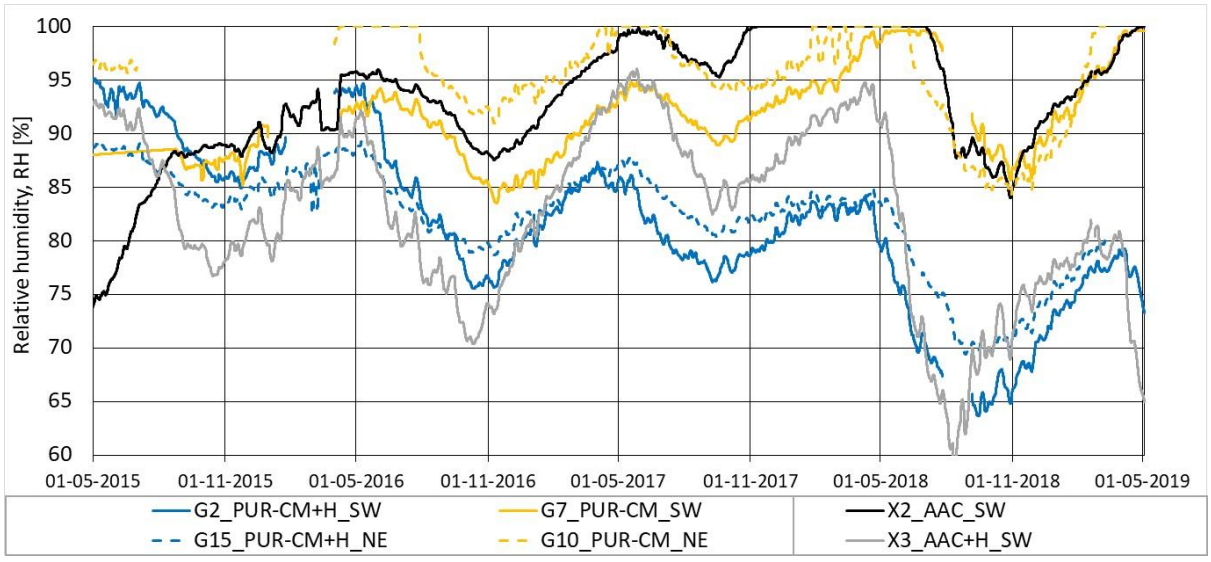

Figure 10 RH in point 5, wall plate

Measurements for the wall plate (Figure 10) showed that exterior hydrophobisation had a positive effect. The PUR-CM+H walls became progressivelt drier. The PUR-CM+H_SW and AAC+H_SW both showed lower RH than their uninsulated reference walls, while the PUR-CM+H_NE showed higher RH than its uninsulated reference wall (see [80]). Hydrophobisation slightly decreased the differences between orientations for the PUR-CM walls.

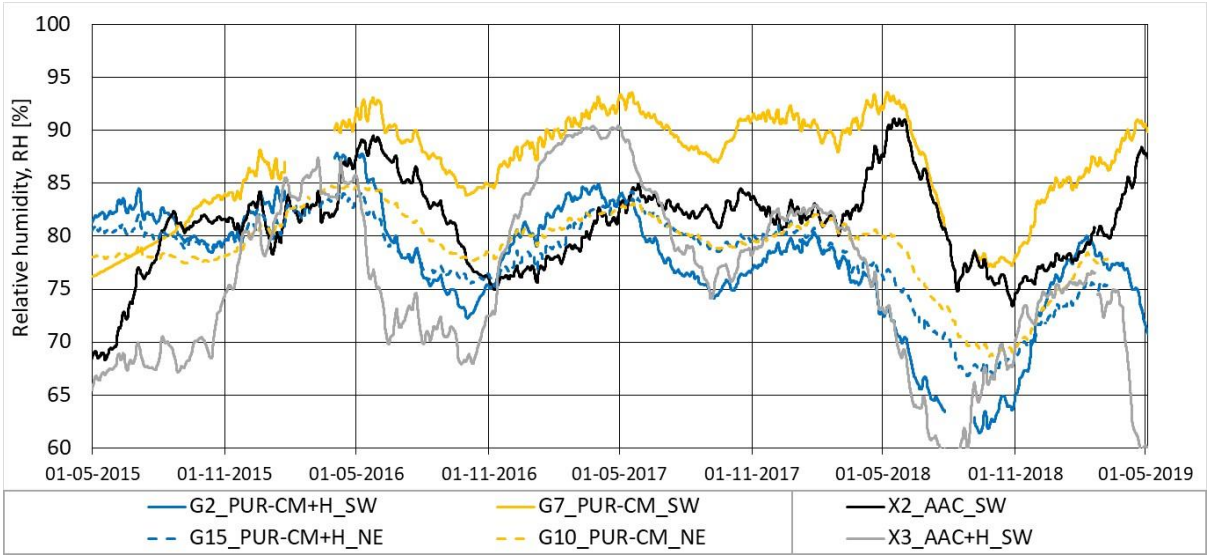

Figure 11 RH in point 6, beam end

Measurements for the beam end (Figure 11) showed that exterior hydrophobisation generally had a positive effect. The PUR-CM+H walls became progressively drier. Large differences were observed between the south-western PUR-CM walls with and without hydrophobisation, compared to the north-eastern PUR-CM walls. The PUR-CM+H showed similar results for both orientations, while the unhydrophobised PUR-CM_NE wall experienced considerably lower RH compared to the unhydrophobised PUR-CM_SW. During the last two years, the PUR-CM+H_SW wall showed similar RH

365 to the AAC+H_SW wall, while without hydrophobisation the PUR-CM_SW wall showed higher RH than
366 the unhydrophobised AAC_SW wall.

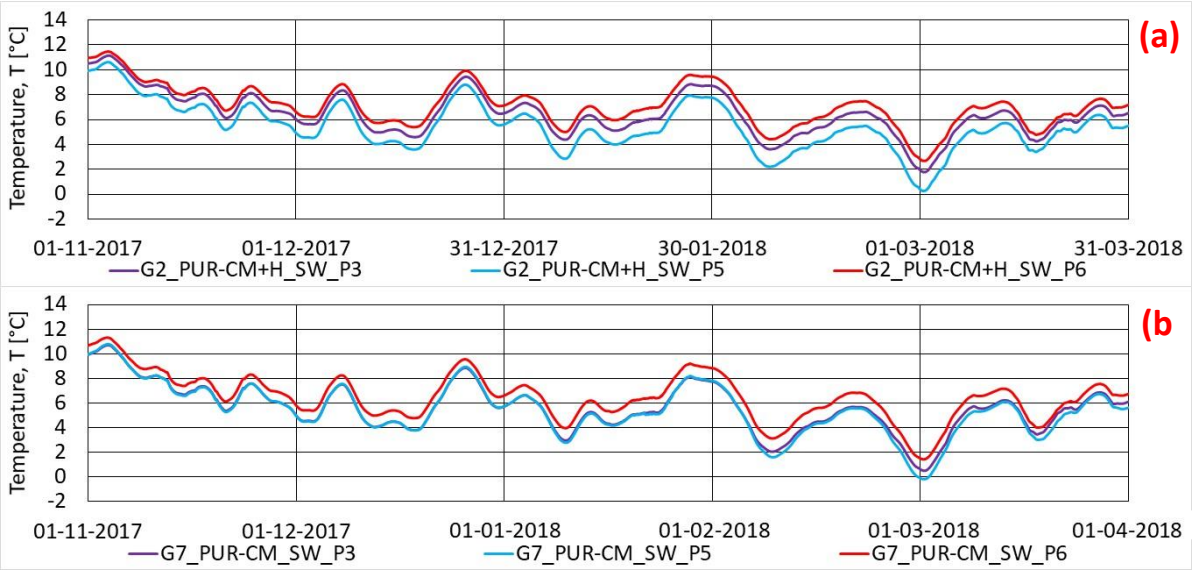

367

368

369 Figure 12 Temperatures in point 3, 5 and 6; interface, wall plate and beam end. South-western PUR-CM wall (a):
370 with hydrophobisation and (b): without hydrophobisation.

371 A comparison between measured temperatures in the interface (point 3), wall plate (point 5) and
372 beam end (point 6) in Figure 12, showed that the beam end was generally the warmest sensor
373 location, and the wall plate the coldest. The exceptions were: 1) the unhydrophobised PUR-CM_SW
374 wall where the interface and wall plate were similar (Figure 12b), and 2) CaSi walls where interface
375 and beam ends were similar, see [80]. The MW and AAC walls showed similar tendencies as the PUR-
376 CM+H_SW wall, see [80].

377

378 **3.2 pH and mould growth**

379 **3.2.1 pH-value**

380 The material tests showed decreasing pH-value for the adhesive mortars and internal lime render for
381 all test walls, except for the PUR-CM walls. The PUR-CM adhesive mortar experienced a slight increase.

382 The lime render behind the PUR-CM system generally maintained a rather high pH-value, except for
383 wall G10. Lime render behind CaSi and AAC mortars showed only slightly higher pH-value than the
384 reference and MW walls.

385 Table 2 pH-values for the adhesive mortars and internal render: fresh, and after 3½ and 4½ years

	Fresh internal lime render	Internal lime render (Nov. 2018)	Internal lime render (Sep. 2019)	Fresh adhesive mortar	Adhesive mortars (Nov. 2018)	Adhesive mortars (Sep. 2019)
G3_Ref_SW	12.7	9.2	9.3			
G14_Ref_NE	12.7		9.2			
X5_Ref_SW	12.7		9.1			
G1_MW_SW	12.7	9.2	9.2			
G2_PUR-CM+H_SW	12.7	12.6	12.0	12.0	12.6	12.5
G7_PUR-CM_SW	12.7	12.7	12.1	12.0	12.5	12.2
G10_PUR-CM_NE	12.7	9.7	12.4	12.0	12.6	12.2
G15_PUR-CM+H_NE	12.7	12.8	12.5	12.0	12.6	12.3
G4_CaSi_SW	12.7	9.5	9.4	12.7	10.2	9.0
G13_CaSi_NE	12.7	9.5	9.3	12.7	10.8	9.2
X2_AAC_SW	12.7	9.4	9.4	12.0	9.7	9.2
X2_AAC+H_SW	12.7	9.4	9.1	12.0	9.5	9.5

386 *pH of lime render was only determined for one of the three reference walls, G3.

387

388 **3.2.2 On-site mould**

389 On-site Mycometer tests (both surface and bulk) showed no mould growth in the PUR-CM and CaSi
390 walls, while mould was found in the MW and AAC walls. Extra test rounds were performed for the AAC
391 system due to the mould findings, and Mycometer surface tests in the interface were generally in the
392 low to medium mould growth range, while the outer bulk-tests were in medium to high mould growth

393 range. The bulk-test results decreased in value towards the interior surface, with no critical results

394 found in the innermost part of the insulation layer.

395 Table 3 Mycometer results for the test walls after 3½, 4 and 4½ years

Test round	Wall ID	Surface test		Bulk-Material test					
				Outer	Outer	Mid	Mid	Inner	Inner
		A	B	A	B	A	B	A	B
1 (Nov. 2018)	G1_MW_SW[1]*	21	BDR	469	159				
	G1_MW_SW (Wood studs)	960	788						
	G2_PUR-CM+H_SW	BDR	BDR	77	32				
	G7_PUR-CM_SW	BDR	BDR	12	27				
	G10_PUR-CM_NE	BDR	BDR	4	89				
	G15_PUR-CM+H_SW	BDR	BDR	BDR	1				
	G4_CaSi_SW	BDR	BDR	BDR	BDR				
	G13_CaSi_NE	BDR	BDR	14	10				
	X2_AAC_SW[1,2]	BDR	41	482	1459	382	390	BDR	7
	X3_AAC+H_SW[1,2]	26	37	43	32				
2 (March 2019)	X2_AAC_SW[2,3,4,6]	141	86	384	254	416	459	6	7
	X3_AAC+H_SW[4,5,6]	26	31	209	410	90	69		
3 (March 2019)	X2_AAC_SW[1,4,5,6]	220	196	824	982	119	98	6	6
	X3_AAC+H_SW[1,2,4]	120	307	585	712	5	3	5	6
4 (Sep. 2019)	G1_MW_SW*	28	13	53	23				
	G1_MW_SW (Wood studs)	35	188						
	G2_PUR-CM+H_SW	3	3	6	5				
	G7_PUR-CM_SW	23	23	9	63				
	G10_PUR-CM_NE	12	9	13	1				
	G15_PUR-CM+H_SW	8	5	10	18				
	G4_CaSi_SW	4	6	9	5				

G13_CaSi_NE	5	5	4	5		
X2_AAC_SW	140	137	332	461	27	24
X3_AAC+H_SW	195	227	450	490	3	24

Mycometer surface tests were taken in the interface, P3 and Mycometer material tests between interface and interior surface, P4. Outer: outermost 10 mm of insulation layer (nearest to the masonry wall); Mid: outermost 11-55 mm (CaSi and AAC) or 11-45 mm (PUR-CM) of insulation layer; Inner: innermost 45 mm (CaSi and AAC) or 35 mm (PUR-CM) of insulation layer. “A” and “B” refer to the two samples taken for each interface and layer of insulation. *Surface samples were taken on the internal render surface and on wooden battens. BDR designates: Below Detection Range. Superscript indicate identified mould species.

Cultivation of the swab tests indicated no growth in the interface, except for walls G1, X2 and X3. The following mould species were identified (see sampling location in Table 3):

- [1]*Aspergillus versicolor*
- [2]*Penicillium chrysogenum*
- [3]*Parengyodontium album (= Tritirachium album = Engyodontium album)*
- [4]*Sarocladium strictum (= Acremonium strictum)*
- [5]*Pseudogymnoascus pannorum* (= *Geomyces pannorum* = *Chrysosporium pannorum*)
- [6]*Cladosporium sphaerospermum*

Photo documentation of mould identification is available in [80].

3.2.3 Mould modelling

The measurements showed that the most critical moisture conditions were to be found in the interface and wall plate, so the mould risk modelling focused on these two locations.

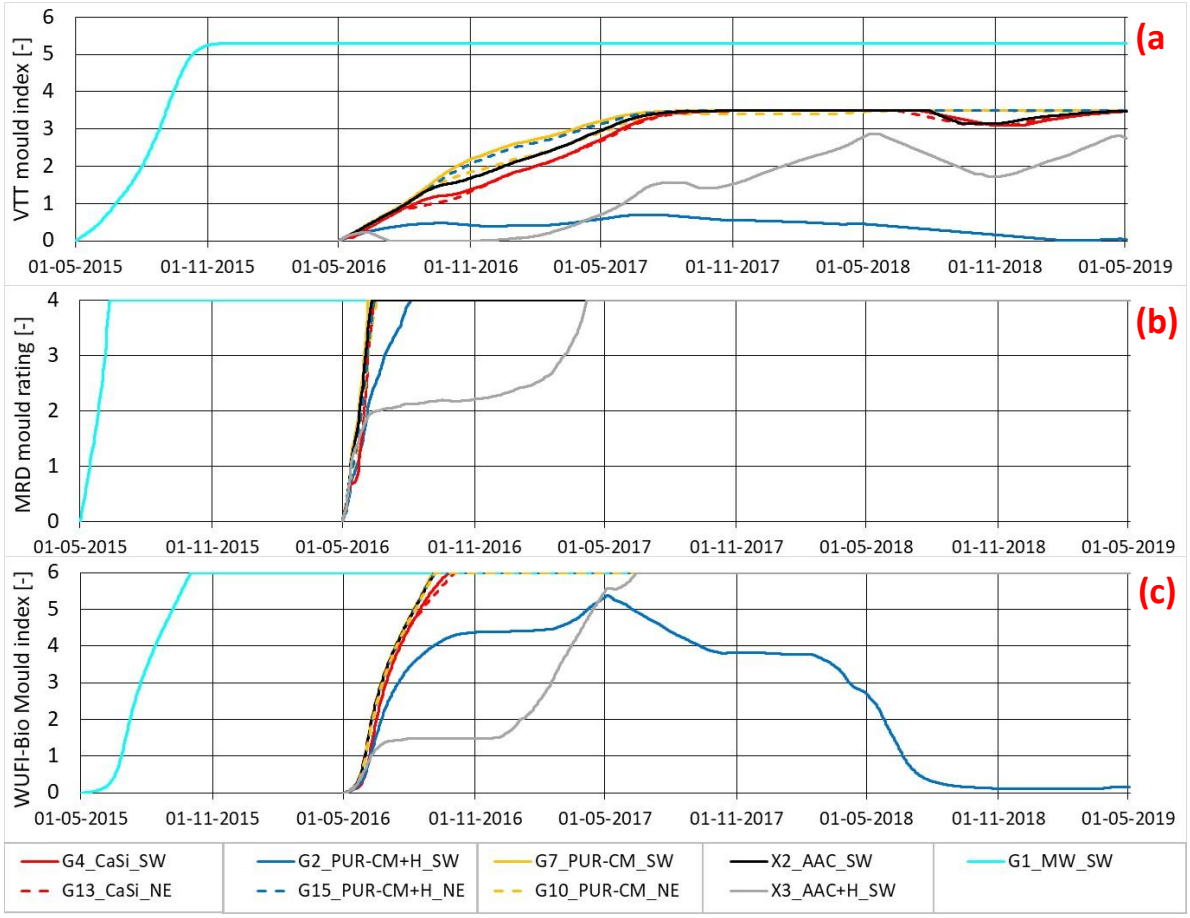

Figure 13 Modelled mould risk at point 3, interface; (a): VTT model, (b): MRD model, and (c): WUFI-Bio. Model predictions were started after one year to emulate the effect of high initial pH-value in the adhesive mortar, except G1 as this wall did not include adhesive mortar.

All mould predictions for the interface (Figure 13) showed high risk for all test walls, except the PUR-CM+H_SW. The different mould-growth models showed large discrepancies for the PUR-CM+H_SW wall. The MDR showed high risk, WUFI-Bio high initial risk followed by a decrease as RH dropped, and VTT no mould risk. Some discrepancies were also observed for the AAC+H_SW. The earlier modelling start for the MW wall was due to not having a high initial pH-value, while the higher index value in the VTT model was due to a more sensitive material class (wood battens); less sensitive materials can at

most reach a VTT mould index of 3.5, while wood, as in the wooden laths in the MW walls can reach 5.3.

The VTT model seemed to best match the observed tendencies for the measurements, so further analysis was performed using the VTT model.

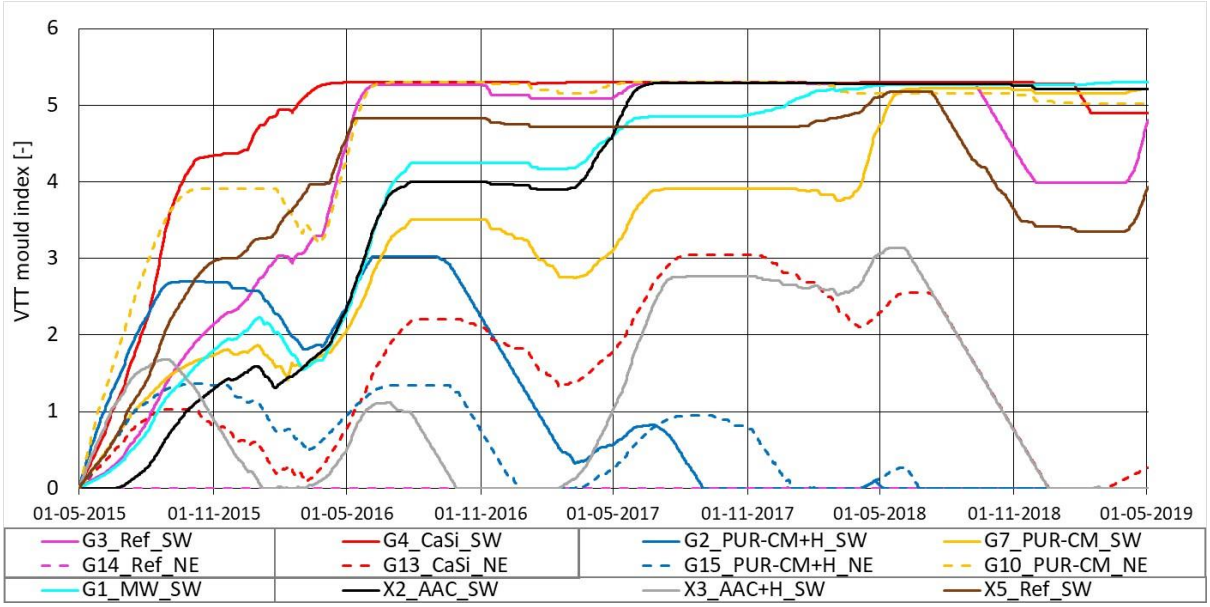

Figure 14 Modelled mould risk in point 5, wall plate.

Mould predictions for the wall plate (Figure 14) showed increasing mould risk tendencies in all test walls, except the PUR-CM+H walls and the north-eastern reference wall. The PUR-CM and AAC systems with hydrophobisation showed considerably lower mould risk than their unhydrophobised counterpart. Moreover, the north-eastern CaSi and reference walls showed considerably lower mould risk than their south-western counterpart. All north-eastern walls were found to have higher mould risk than their reference wall.

445

446

447

448 ### 3.3 Summary of key results

449 Table 4 presents a summary of key results for moisture, predicted- and on-site mould growth.

450 Table 4 Key summary results

Sensor locations P3: Interface P4: Interior surface P5: Wall plate P6: Beam end	Average RH [%]				Max VTT MI [-]		Average MI [-]		Mycometer surface results [MV]			
	P3	P4	P5	P6	P3	P5	P3	P5	Test1 P3	Test2 P3	Test3 P3	Test4 P3
G3_Ref_SW		78.4	91.9	82.3		5.3		4.3				
G14_Ref_NE		77.9	70.1	80.5		0		0				
X5_Ref_SW		78.5	90.7	78.7		5.2		4.0				
G1_MW_SW	99.4	74.9	94.6	92.9	5.3	5.3	4.9	3.9				
G2_PUR-CM+H_SW	88.1	67.8	81.6	77.7	0.7	3.0	0.4	1.1	BDR			BDR
G7_PUR-CM_SW	99.9	66.5	91.2	86.7	3.5	5.2	3.0	3.4	BDR			BDR
G10_PUR-CM_NE	97.8	67.5	95.9	79.1	3.5	5.3	2.8	4.7	BDR			BDR
G15_PUR-CM+H_NE	99.9	68.6	82.3	78.1	3.5	1.4	2.9	0.5	BDR			BDR
G4_CaSi_SW	96.8	66.9	97.6	88.9	3.5	5.3	2.7	4.9	BDR			BDR
G13_CaSi_NE	96.5	68.1	85.3	83.6	3.5	3.1	2.7	1.5	BDR			BDR
X2_AAC_SW	96.6	71.7	93.2	81.1	3.5	5.3	2.8	3.8	41	141	220	140
X3_AAC+H_SW	89.7	68.8	82.6	75.9	2.9	3.1	1.4	1.2	37	31	307	227

451 *Average values are based on the entire four-year data set. The colour codes used for the VTT results are from

452 [78]. BDR designates: Below Detection Range.

453

4 Discussion

4.1 System comparison (non-hydrofobised walls)

Interior surface (Figure 5): Compared to the uninsulated reference walls, the diffusion-open capillary active systems increased the interior surface temperature, which reduced RH levels of the interior surface. The tight MW system did however show different tendencies, showing considerably lower RH during winter compared to the diffusion-open capillary systems, followed by a drastic increase in RH during the summer period. The tendencies indicate that: 1) the vapour barrier was correctly installed, preventing outwards moisture transport; and 2) the occurrence of an inward moisture flow condensing on the exterior side of the vapour barrier (summer condensation) as described in [17], [18], [23]. This did not occur for the other systems, probably due to their diffusion-open nature.

Masonry/insulation interface: After installation of the internal insulation, the interior masonry surface became colder, which increased the RH levels in the interface (Figure 6). For the highly diffusion-open AAC or CaSi systems, inward diffusion drying was observed in summer while outward wetting occurred in winter causing moisture saturation. The CaSi and AAC systems were seen to respond faster to changes in the boundary conditions compared with the tighter MW and PUR-CM, resulting in occasions with lower RH. This effect can be seen in a comparison of the summers of 2016 and 2018. Summer 2018 was abnormally warm and dry, causing a major drop in RH levels for the CaSi and AAC systems, compared to the more rainy and cold summer 2016. During the same periods, the south-western MW and PUR-CM walls were rather stable near 100% RH. The poor performance of the MW and PUR-CM systems was probably caused by inward moisture flow condensing inside the wall, due to the tight nature of the systems. For the CaSi and AAC systems the issue was probably a sub-optimal combination of highly permeable insulation and high indoor moisture load, resulting in condensation in the interface during winter, and lack of exterior rain protection. The nature of the diffusion-open systems was intended to allow for inward drying, however these systems were shown to be near 100% RH in the interface throughout most of the measurement period. Findings for the

diffusion-open systems support those of [36]–[38]. Furthermore, in line with the present findings, [25], [39] found diffusion-open systems to perform slightly better than the diffusion-tight systems when WDR was an issue, and [25], [40] suggested that tighter systems would perform better if WDR was eliminated.

Wall plate (Figure 7): The interior insulation increased the RH levels as the temperature decreased and inward drying was reduced. It was observed that wetting of the wall plates occurred during summer due to solar driven inward moisture transfer while drying was observed during winter, which shows the changes in direction of the vapour flow over the year. These tendencies were observed also for the beam ends. In the south-west orientation the more diffusion-tight and/or less capillary active systems (MW, PUR-CM and AAC) performed better than the more diffusion-open and capillary active CaSi system. MW, PUR-CM and AAC all experienced slowly increasing RH with similar tendencies throughout the experiment just offset some 5-8% point in relation to each other, while the CaSi system rapidly increased to almost 100% RH. Large differences were observed between the unhydrophobised south-western AAC and CaSi walls, despite rather similar measured WDR (see [80]) and material properties (except for thermal conductivity and water absorption). The higher moisture levels for the CaSi systems was probably caused by the sub-optimal combination of no rain protection and highly diffusion-open and capillary active material properties allowing for more moisture diffusion during winter periods, as well as a higher moisture storage capacity. Comparison between the wall plates in the CaSi and PUR-CM walls facing the south-west orientation showed only minor differences in the measured temperatures ($\Delta T<0.5$ °C) between the walls, which suggests that the increased RH levels observed in the CaSi wall would be the result of the moisture transport properties of the system. A slightly larger difference was observed to the AAC wall, however this may also be due to the slight differences in the indoor boundary conditions between the two containers.

Beam end (Figure 8): PUR-CM and CaSi deviated from the reference wall by +8% RH and AAC within ±5% RH, with some larger peaks in the summer. In the south-west orientation, the insulation in PUR-CM and CaSi walls increased RH levels, and for the PUR-CM system the high RH levels were probably

505 caused by reduced inward drying combined with a higher rain load on the exterior surface. The main
506 issue for the CaSi system would probably be outward diffusion during winter. The AAC system showed
507 rather similar levels as the uninsulated reference wall. The tight MW system seemed to have
508 tendencies similar to those of the semi diffusion-tight south-western PUR-CM wall, however with
509 slight higher RH levels, probably due to the reduced inward drying caused by the vapour barrier. These
510 results do not support those of [42], [43], who both found more critical moisture levels in the beam
511 ends of more diffusion-open, compared to more diffusion-tight systems (MW with vapour barrier).
512 However, these studies were carried out with exterior rain protection [42] or as a hot-box cold-box
513 experiment without driving rain [43].

514 The beam end was observed to be in a less critical situation than the wall plate, probably due to the
515 beam end being in the centre of the thermal bridge created by the floor structure, while the wall plate
516 was covered by the insulation system. In addition, the installed wall plate sensor was horizontally
517 located some 200 mm away from the beam end, with mineral wool (emulating the pugging layer)
518 installed inside the floor structure that may have further reduced the heat flow to the wall plate. This
519 would mean the beam end received more heat, causing higher temperatures compared to the wall
520 plate (which Figure 12 corroborates). Furthermore, the beam had a larger potential for moisture
521 redistribution to the indoor environment, compared with the wall plate, which had very limited
522 possibilities.

523 **4.2 Effect of orientation (non-hydrofobised walls)**

524 **Interior surface (Figure 5)**:

525 The higher WDR load and solar irradiation from the south-west orientation in comparison to the north-
526 east orientation were found to have limited or no effect on the RH levels and temperatures near the
527 interior surface of the reference wall and insulated walls.

528 **Masonry/insulation Interface (Figure 6):**

529 The south-west facing wall with CaSi experienced only slightly increased RH levels and temperatures
530 in the interface compared to the north-east facing wall, while the south-west facing PUR-CM wall
531 experienced a large increase in the RH levels compared with its north-eastern counterpart. The results
532 suggest that the increased WDR load from south-west had little effect on the hygrothermal
533 performance of the CaSi walls due the high vapour and liquid permeability of the system which
534 allowed for rapid inward drying. In contrast, the large increase in RH levels for the south-west facing
535 PUR-CM wall was probably the result of the tight nature of the insulation systems with very limited
536 moisture transport.

537 **Wall plate (Figure 7)**:

538 The north-east facing reference wall and CaSi wall experienced progressively decreasing RH, opposite
539 to their south-west facing counterparts which showed progressively increasing RH caused by the
540 higher rain load from south-west, suggesting that rain protection may be necessary. Regarding the
541 two PUR-CM walls, the observed lower RH levels in the south-west orientation compared to the north-
542 east oriented wall could perhaps be due to increased drying from higher solar exposure. However,
543 later in the test period both PUR-CM walls showed similar RH levels. The results indicate that in the
544 case of low rain load and solar radiation on the wall (north-east orientation), the semi-tight PUR-CM
545 system performed worse than the CaSi system. However, with a larger rain load and solar exposure
546 from south-west the CaSi system showed increased RH levels compared with the PUR-CM system,
547 perhaps also caused by the increased outwards vapour diffusion during winter.

548 **Beam end (Figure 8)**:

549 The effects of the north-east orientation on the embedded wooden beam ends were generally seen
550 to be similar to the observed effects on the embedded wooden wall plates. However, the differences
551 between orientations were seen to be smaller which was probably caused by the increased heat flow
552 passing through the beam ends compared with the wall plates.

553

4.3 Effect of hydrophobisation

The results indicate that hydrophobisation generally had a positive effect on the hygrothermal performance of the wall with PUR-CM and AAC, although the effect differed considerably between the two systems. The more diffusion-tight PUR-CM system showed decreasing tendencies in all sensor locations, except for interface and beam end in the north-eastern PUR-CM wall. For the highly diffusion-open AAC system, hydrophobisation improved the hygrothermal conditions in all locations compared to the unhydrophobised AAC wall. However, high RH levels were still observed in both the interface and the wall plate. In the interface the hydrophobisation caused a considerable reduction in RH levels during summer as rain intrusion was reduced considerably, followed by a rapid increase during the following winter period. The results indicate that this was due to the highly diffusion-open nature of the AAC system, allowing more outward moisture diffusion from the indoor climate during winter. This resulted in more interstitial condensation. Results for the effect of hydrophobisation together with diffusion-open and –tight systems support the findings in [37], [38].

For the semi-tight PUR-CM walls, the effect of hydrophobisation varied with the orientation. In the south-west orientation, all three sensor locations showed a large reduction as a result of hydrophobisation. In the north-east orientation, a reduction was seen only for the wall plate, while interface and beam end showed similar RH levels with and without hydrophobisation. This indicates that the small reduction of rain load due to hydrophobisation is only observable at the wall plate which is closer to the outside compared with the interface (80-90 mm). The beam end is even closer to the outside but the effect of the thermal bridge may outweigh the effect of reduced rain load. In line with the present findings for interface in the north-east facing walls, [53] found little or no benefit of hydrophobisation on a well-protected solid masonry wall.

4.4 pH-value

The pH measurements in the interface correlate with the water vapour permeability of the insulation system: systems with higher permeability (CaSi and AAC) experienced lower adhesive mortar pH-value over time compared to the more diffusion-tight systems (PUR-CM), as CO_2 from the surrounding environment would have easier access to the adhesive mortar and internal lime render. The PUR-CM adhesive mortar increased pH-value compared to the fresh adhesive mortar samples, probably because the higher pH-value of the internal lime render affected the adhesive mortar by a washing out process, with the exception of wall G10. The value for G10 was the average of four samples, perhaps due to a local divergence.

4.5 On-site mould

No mould growth was detected in the PUR-CM and CaSi systems using the Mycometer method. This was most likely due to the high pH-value (initial 12 and 12.7 respectively, and 12.2-12.5 and 9-9.2 after 4½ years) in the adhesive mortar combined with little or no available nutrients, which created an unfavourable growth environment that prevented mould growth for at least 4½ years, even in the case of the high RH levels that were observed for the unhydrophobised walls. In contrast, mould growth was detected in the AAC system, probably due to a low pH-value (initial 12, and 9.2-9.5 after 4½ years) in the interface and contrary to the CaSi, there seemed to be available nutrition in the insulation system allowing for a more favourable growth environment in the outermost part of the insulation layer and interface where high RH levels were observed. Less growth was observed in the interface compared to the outermost and central parts of the insulation layer, perhaps because of the high initial pH-value (ca. 12) of the adhesive mortar that created an unfavourable growth environment in the interface. The bulk-test results suggest that mould can grow through the pores of the insulation material, possibly due to the coarse pore structure of the AAC. Given enough time and moisture the growth could potentially affect the indoor environment and become a problem. High growth was also

601 found in the MW system. This was, however, expected considering the neutral pH, high RH levels and
602 the nutrition provided by the wooden battens.

603 In correlation with the Mycometer results, the cultivation of swab tests on V8 and DG18 media showed
604 no growth in the interface for the PUR-CM and CaSi systems while mould was detected in the MW and
605 AAC systems. The identified species in the MW and AAC systems were species typically found in water-
606 damaged buildings, growing on wooden and concrete elements [62], [81]–[83]. The lack of mould
607 growth in the PUR-CM and CaSi systems were perhaps due to high pH-value over an extended period
608 making spores unable to germinate or killing them.

609 **4.6 Mould modelling**

610 Comparison between models (in the interface) showed a general agreement between the three
611 models for test walls with very high RH levels. The main differences seemed to be related to growth
612 speed, the rating scale that was used and for the VTT model a "level cap" related to the material
613 sensitivity. However, the modelling results varied greatly for the south-western PUR-CM and AAC walls
614 with hydrophobisation which had medium high RH levels. These discrepancies can be caused by the
615 choice of different definitions for growth conditions: MDR, $RH_{crit} \geq 75\%$; WUFI-Bio Class 2 (PUR and
616 concrete), $RH_{crit} \geq 79\%$ (temperature dependent); VTT class 3 (PUR and concrete), $RH_{crit} \geq 85\%$
617 (temperature dependent).

618 Comparison between modelled and on-site mould showed little correlation, as no mould was found,
619 neither by cultivation nor by Mycometer tests, in 9 out of 12 test walls, probably due to the high initial
620 pH-values. High pH-value was not included in the models as a factor, but was stated in [78], [84] to
621 potentially hamper growth during the initial period. The first year was assumed to be the initial period.
622 However, for some of the walls the high pH lasted for at least 4½ years. Moreover, while the models
623 did take material resistance into consideration (for determination of critical RH level or time to onset
624 of mould growth), they also assumed growth would inevitably occur whenever the correct
625 temperature and RH levels were present, an assumption that may not be correct for tightly closed

626 structure without available nutrition, and no introduction of dust, dirt and spores from the
627 surroundings.

628 The reliability of some of the available models was assessed in [69], [84]–[88], which found that the
629 models cannot precisely predict the extent of the growth, but rather the possibility of mould growth.
630 Similarly, in [89] it was found that real growth does not always follow mould predictions, even when
631 there are favourable conditions. Discrepancies between real and modelled growth include: insufficient
632 knowledge regarding the possibility of mould growth on different materials and on the effect of ageing
633 [90]; use of incubation conditions as surfaces [85], [86]; different or incorrect definitions of
634 germination start and time, and of growth conditions [84]–[86]; differences in inoculation techniques
635 and added spore concentration [85], [86]. Gradeci et al. [91] proposed instead a probabilistic-based
636 approach for predicting mould growth.

637 Despite questionable reliability for precise mould predictions, models are still useful tools for assessing
638 the combined hygrothermal conditions over time, and for comparing different design scenarios.

639 **4.7 Indoor moisture load**

640 Note that while an indoor RH of 60% may be appropriate during the Danish summer, it would be high
641 for the Danish winter. In [17], [92] 30-50% is suggested as more appropriate during winter. The intent
642 of the present study was to test the insulation systems under the harder conditions of the highest
643 humidity class for residential buildings. A reduction of the indoor RH levels would certainly reduce
644 potential risks at certain locations due to a reduced potential for diffusion through the diffusion-open
645 systems assessed in this study.

646 In addition, the experiment was carried out using two conditioned containers, each slightly different
647 in indoor RH and temperature boundary conditions. These differences may have intermittently biased
648 the results for some systems, but have probably not affected the general conclusions.

4.8 Measurement equipment

It was expected that the embedded sensors may deviate over time due to aging, however it was not practically possible to take out and re-calibrate all the sensors. Control measurements were instead performed with wooden dowels embedded in a few locations in the masonry walls, which indicated that some sensors could potentially overestimate the RH levels by up to 5-7%-point during periods with near 100% RH, while good correlations were observed for lower RH levels.

5 Conclusions

This paper presented a 4 year field study of 24 solid masonry walls with embedded wooden elements and internal insulation. The hygrothermal performance of three diffusion-open capillary insulation systems was assessed, and the risk of mould growth was determined from mathematical models and by on-site testing. The effect of exterior hydrophobisation was also investigated. In addition to observing that high indoor RH in the winter causes high RH behind interior insulation, and that the level is dependent on the diffusion tightness of the insulation material, the findings show:

- With exterior hydrophobisation the more diffusion-tight systems performed better compared to the diffusion-open systems. Without hydrophobisation, the diffusion-open systems performed slightly better, as they are less sensitive to summer condensation.
- The effect of hydrophobisation was shown to vary with the facade orientation for the semi-tight PUR-CM system, as RH levels were reduced considerably in all three locations in the south-west oriented wall while for the north-east oriented wall the effect differed considerably between locations. The discrepancies between orientations may be due to differences in rain load and solar exposure, affecting the potential benefit from the exterior hydrophobisation. For the locations, the observed variations may be due to differences in heat and diffusion from the indoor environment.

- Less critical moisture levels and mould risk were achieved for the interface between masonry wall and the insulation system, and for embedded wooden elements, using the PUR-CM system in combination with exterior hydrophobisation.
- The combination of little or no available nutrition and high initial pH-value in the adhesive mortar probably created unfavourable germination and growth conditions and prevented mould growth for an extended period in the PUR-CM and CaSi systems. Growth was however found in walls with AAC insulation, which like the CaSi system was found to have a low pH-value, but unlike the CaSi system, the AAC systems likely contained some form of available nutrition.
- Poor correlation was found between modelled and on-site mould growth. The results indicate that mould-growth models overestimate the risk. The discrepancies may have occurred because little or no nutrition was available in the materials tested and because the adhesive mortars that were used had high pH-values, hampering growth, a factor not encompassed by the used mould-growth models.
- Practical implications from the study: RH levels may be reduced through the application of exterior hydrophobisation and it seems to be a necessary measure for the examined systems to maintain less critical RH levels.
- When combined with exterior hydrophobisation, the findings indicate that the more diffusion-tight insulation systems are to be preferred over the highly diffusion-open systems.
- The risk of mould growth in the critical locations may be reduced considerably by application of the insulation systems using high pH (>12) adhesive mortar, even if the relative humidity is high. The more diffusion-tight systems seem to better maintain the high pH. Furthermore, no organic residues or parts should be available in the critical locations, especially if there is a risk of a fast decline in pH.

6 Acknowledgment

The authors would like to thank the companies Byggros, and Intro Flex for installation of their insulation systems, and Intro Flex for application of Remmers Funcosil FC on the exterior surface.

The participating companies have had no influence on the results and analyses presented in this paper.

This research was financially supported by Grundejernes Investeringsfond (The Landowners' Investment Foundation), Realdania and the European Union's Horizon 2020 research and innovation programme under grant agreement No 637268 – as part of the RIBuild project.

7 References

[1] H. Tommerup and S. Svendsen, "Energy savings in Danish residential building stock," *Energy Build.*, vol. 38, pp. 618–626, 2006.

[2] K. B. Wittchen, "SBi 2009:05 Potentielle energibesparelser i det eksisterende byggeri (Danish)," Danish Building Research Institute, Hørsholm, Denmark, 2009.

[3] K. B. Wittchen, J. Kragh, and O. M. Jensen, "Energy-saving potential – a case study of the Danish building stock," in *Proceeding at eceee 2011 summer study - Energy Efficiency First: the Foundation of a Low-carbon Sociey*, 2011, pp. 1355–1363.

[4] J. Kragh and K. B. Wittchen, "Development of two Danish building typologies for residential buildings," *Energy Build.*, vol. 68, pp. 79–86, 2014.

[5] T. Odgaard, S. P. Bjarløv, and C. Rode, "Interior insulation—Characterisation of the historic, solid masonry building segment and analysis of the heat saving potential by 1d, 2d, and 3d simulation," *Energy Build.*, vol. 162, pp. 1–11, 2018.

[6] G. R. Finken, S. P. Bjarløv, and R. H. Peuhkuri, "Effect of façade impregnation on feasibility of capillary active thermal internal insulation for a historic dormitory - A hygrothermal simulation

721 study," *Constr. Build. Mater.*, vol. 113, pp. 202–214, 2016.

722 [7] M. Morelli and S. Svendsen, "Investigation of interior post-insulated masonry walls with
723 wooden beam ends," *J. Build. Phys.*, vol. 36, no. 3, pp. 265–273, 2013.

724 [8] N. F. Jensen, "Hygrothermal Analysis of Retrofitted Buildings in the Campus of Lund University,"
725 Lund University, 2016.

726 [9] P. Häupl, K. Jurk, and H. Petzold, "Inside thermal insulation for historic facades," *Res. Build.*
727 *Phys.*, pp. 463–469, 2003.

728 [10] J. Toman, A. Vimmrová, and R. Černý, "Long-term on-site assessment of hygrothermal
729 performance of interior thermal insulation system without water vapour barrier," *Energy*
730 *Build.*, vol. 41, pp. 51–55, 2009.

731 [11] M. Harrestrup and S. Svendsen, "Full-scale test of an old heritage multi-storey building
732 undergoing energy retrofitting with focus on internal insulation and moisture," *Build. Environ.*,
733 vol. 85, pp. 123–133, 2015.

734 [12] M. Morelli, L. Rønby, S. Erik, M. G. Minzari, T. Kildemoes, and H. M. Tommerup, "Energy
735 retrofitting of a typical old Danish multi-family building to a ' nearly-zero ' energy building
736 based on experiences from a test apartment," *Energy Build.*, vol. 54, pp. 395–406, 2012.

737 [13] P. Johansson, S. Geving, C. Hagentoft, B. Petter, and E. Rognvik, "Interior insulation retro fi t of
738 a historical brick wall using vacuum insulation panels : Hygrothermal numerical simulations and
739 laboratory investigations," *Build. Environ.*, vol. 79, pp. 31–45, 2014.

740 [14] P. Klõšeiko, E. Arumägi, and T. Kalamees, "Hygrothermal performance of internally insulated
741 brick wall in cold climate: A case study in a historical school building," *J. Build. Phys.*, vol. 38,
742 no. 5, pp. 444–464, 2014.

743 [15] E. Biseniece, G. Žogla, A. Kamenders, R. Purviņš, K. Kašs, and R. Vanaga, "Thermal performance
744 of internally insulated historic brick building in cold climate: A long term case study," *Energy*

745 *Build.*, vol. 152, pp. 577–586, 2017.

746 [16] M. Morelli and E. B. Møller, “Energy Savings and Risk of Mold Growth in Apartments Renovated
747 with Internal Insulation (Accepted Manuscript),” *Sci. Technol. Built Environ.*, 2019.

748 [17] E. Brandt, T. Bunch-Nielsen, G. Christensen, C. Gudum, M. H. Hansen, and E. B. Møller, *SBi-*
749 *Anvisning 224 - Fugt i Bygninger (Danish)*, 2nd ed. Hørsholm, Denmark: Statens
750 Byggeforskningensinstitut, Aalborg University, 2013.

751 [18] J. Straube and C. Schumacher, “Interior insulation retrofits of load-bearing masonry walls in
752 cold climates,” *J. Green Build.*, vol. 2, no. 2, pp. 42–50, 2007.

753 [19] P. Mensinga, J. Straube, and C. Schumacher, “Assessing the Freeze- Thaw Resistance of Clay
754 Brick for Interior Insulation Retrofit Projects,” in *Proceedings of Thermal Performance of the*
755 *Exterior Envelopes of Whole Buildings Xi International Conference*, 2010.

756 [20] K. Ueno and J. Straube, “Field Monitoring and Simulation of a Historic Mass Masonry Building,”
757 in *Proceedings of Thermal Performance of the Exterior Envelopes of Whole Buildings XI*, 2013.

758 [21] C. Gorse and D. Highfield, *Refurbishment and upgrading of buildings 2nd Edition*. New York,
759 USA: Taylor & Francis, 2009.

760 [22] J. Munch-Andersen, *SBi-anvisning 221: Efterisolering af etageboliger (Danish)*. Hørsholm,
761 Denmark: Statens Byggeforskningensinstitut, Aalborg University, 2008.

762 [23] H. M. Künzel, “Effect of interior and exterior insulation on the hygrothermal behaviour of
763 exposed walls,” *Mater. Struct.*, vol. 31, no. 2, pp. 99–103, 1998.

764 [24] J. Zhao, J. Grunewald, U. Ruisinger, and S. Feng, “Evaluation of capillary-active mineral
765 insulation systems for interior retrofit solution,” *Build. Environ.*, vol. 115, pp. 215–227, 2017.

766 [25] E. Vereecken, L. Van Gelder, H. Janssen, and S. Roels, “Interior insulation for wall retrofitting –
767 A probabilistic analysis of energy savings and hygrothermal risks,” *Energy Build.*, vol. 89, pp.
768 231–244, 2015.

[26] G. Christensen, A. P. Koch, and E. B. Møller, “Indvendig efterisolering - ældre ydervægge af murværk (Danish),” Copenhagen, Denmark, 2015.

[27] H. Viitanen *et al.*, “Moisture and biodeterioration risk of building materials and structures,” *J. Therm. Envel. Build. Sci.*, vol. 33, no. 3, pp. 201–224, 2010.

[28] A. G. Wilson, “Condensation in insulated masonry walls in summer,” in *RILEM/CIB Symposium Moisture Problems in Buildings, Helsinki, Finland*, 1965.

[29] G. Scheffler and J. Grunewald, “Material development and optimisation supported by numerical simulation for a capillary-active inside insulation material,” *Res. Build. Phys.*, pp. 77–85, 2003.

[30] V. Kočí, J. Maděra, and R. Cerný, “Computer aided design of interior thermal insulation system suitable for autoclaved aerated concrete structures,” *Appl. Therm. Eng.*, vol. 58, pp. 165–172, 2013.

[31] Z. Pavlík and R. Černý, “Experimental assessment of hygrothermal performance of an interior thermal insulation system using a laboratory technique simulating on-site conditions,” *Energy Build.*, vol. 40, pp. 673–678, 2008.

[32] Z. Pavlík and R. Černý, “Hygrothermal performance study of an innovative interior thermal insulation system,” *Appl. Therm. Eng.*, vol. 29, pp. 1941–1946, 2009.

[33] V. Marincioni and H. Altamirano-Medina, “Effect of orientation on the hygrothermal behaviour of a capillary active internal wall insulation system,” in *Proceedings of the 10th Nordic Symposium on Building Physics, NSB 2014, Lund, Sweden*, 2014, pp. 1238–1243.

[34] P. Wegerer, J. Nathanael, and T. Bednar, “Measuring the Hygrothermal Performance of an Interior Insulation made of Woodfibre Boards - The 6th International Building Physics Conference, IBPC 2015,” in *Energy Procedia*, 2015, vol. 78, pp. 1478–1483.

[35] T. Odgaard, S. P. Bjarløv, and C. Rode, “Interior insulation – Experimental investigation of

hygrothermal conditions and damage evaluation of solid masonry façades in a listed building," *Build. Environ.*, vol. 129, pp. 1–14, 2018.

[36] G. A. Scheffler, "Hygric performance of internal insulation with light-weight autoclaved aerated concrete," in *Proceeding of 5th Int. Conf. Autoclaved Aerated Concrete, September 15-16, 2011, Bydgoszcz, Poland*, 2011, pp. 323–335.

[37] T. Odgaard, S. P. Bjarløv, and C. Rode, "Influence of hydrophobation and deliberate thermal bridge on hygrothermal conditions of internally insulated historic solid masonry walls with built-in wood," *Energy Build.*, vol. 173, pp. 530–546, 2018.

[38] N. F. Jensen and S. P. Bjarløv, "GI slutrapport – Anvendelighed og robusthed af indvendig efterisolering (Danish)," Kgs. Lyngby, Denmark, 2019.

[39] T. De Mets, A. Tilmans, and X. Loncour, "Hygrothermal assessment of internal insulation systems of brick walls through numerical simulation and full-scale laboratory testing - The 11th Nordic Symposium on Building Physics," in *Energy Procedia*, 2017, vol. 132, pp. 753–758.

[40] E. Vereecken and S. Roels, "A comparison of the hygric performance of interior insulation systems: A hot box – cold box experiment," *Energy Build.*, vol. 80, pp. 37–44, 2014.

[41] T. K. Hansen, S. P. Bjarløv, R. H. Peuhkuri, and M. Harrestrup, "Long term in situ measurements of hygrothermal conditions at critical points in four cases of internally insulated historic solid masonry walls," *Energy Build.*, vol. 172, pp. 235–248, 2018.

[42] P. Kopecký, J. Tywoniak, and J. Richter, "Experimental investigations of wooden beam ends in masonry with internal insulation - The 11th Nordic Symposium on Building Physics, NSB2017," in *Energy Procedia*, 2017, vol. 132, pp. 682–687.

[43] E. Vereecken and S. Roels, "Wooden beam ends in combination with interior insulation : An experimental study on the impact of convective moisture transport," *Build. Environ.*, vol. 148, pp. 524–534, 2019.

[44] M. Morelli, G. A. Scheffler, T. R. Nielsen, and S. Svendsen, “Internal Insulation of Masonry Walls with Wooden Floor Beams in Northern Humid Climate,” in *Proceedings of Thermal Performance of the Exterior Envelopes of Whole Buildings XI International Conference, clearwater, Florida, USA*, 2010.

[45] E. Vereecken and S. Roels, “Capillary active interior insulation: do the advantages really offset potential disadvantages?,” *Mater. Struct.*, vol. 48, pp. 3009–3021, 2015.

[46] A. Nielsen, E. B. Møller, T. V Rasmussen, and E. J. D. P. Hansen, “Use of sensitivity analysis to evaluate hygrothermal conditions in solid brick walls with interior insulation,” in *In Proceedings of the 5th International Building Physics Conference (IBPC): The Role of Building Physics in Resolving Carbon Reduction Challenge and Promoting Human Health in Buildings, Kyoto, Japan*, 2012, pp. 377–384.

[47] J. Macmullen, Z. Zhang, E. Rirsch, H. Nath, and N. Bennett, “Brick and mortar treatment by cream emulsion for improved water repellence and thermal insulation,” *Energy Build.*, vol. 43, no. 7, pp. 1560–1565, 2011.

[48] E. Rirsch, “Energy Saving from Water Repellents,” in *Proceedings of Salford Retrofit 2012 conference, University of Salford Manchester*, 2012.

[49] T. K. Hansen, S. P. Bjarløv, R. H. Peuhkuri, and K. K. Hansen, “Performance of hydrophobized historic solid masonry – Experimental approach,” *Constr. Build. Mater.*, vol. 188, pp. 695–708, 2018.

[50] S. Couto, T. D. Goncalves, and J. M. G. Lopes, “Drying of Red Ceramic Brick. Effect of five Silicone-based Water-Repellent Treatments,” in *Proceedings of Hydrophobe VI The 6th International Conference on Water Repellent Treatment of Building Materials, Rome, Italy*, 2011, pp. 81–92.

[51] M. Roos, F. König, S. Stadtmüller, and B. Weyershausen, “Evolution of Silicone Based Water

Repellents for Modern Building Protection," in *Proceedings of Hydrophobe V The 5th International Conference on Water Repellent Treatment of Building Materials, Brussels, Belgium*, 2008, vol. 16, pp. 3–15.

[52] M. Harrestrup and S. Svendsen, "Internal insulation applied in heritage multi-storey buildings with wooden beams embedded in solid masonry brick façades," *Build. Environ.*, vol. 99, pp. 59–72, 2016.

[53] H. M. Künzel and K. Kießl, "Drying of brick walls after impregnation," *Bauinstandsetzen*, vol. 2, pp. 87–100, 1996.

[54] J. C. Zak and H. G. Wildman, "Fungi in Stressful Environments," in *Biodiversity of Fungi: Inventory and Monitoring Methods*, Elsevier, 2004, pp. 303–315.

[55] Byggros A/S, "Calsitherm Indeklimaplade Brochure (Danish)," 2017. [Online]. Available: https://mediacache3.bgflux.com/c0/49/0b51-f950-4a4e-8876-fa6e16d6c2bc/brochure calsitherm indeklimaplade.pdf. [Accessed: 15-Aug-2019].

[56] Ytong Multipor, "Ytong Multipor til indvendig efterisolering: Projektering indvendig efterisolering (Danish)," 2013. [Online]. Available: http://www.mureraarhus.dk/CustomerData/Files/Folders/3-pdf/19_indvendig-efterisolering-2.pdf. [Accessed: 15-Aug-2019].

[57] Remmers Gmbh, "Systemer til skimmelsanering (Danish)," 2018. [Online]. Available: https://www.introflex.dk/images/skimmelsvamp/1018_SCHIMMEL-SANIERUNG_2018_DK_HK3-003.pdf. [Accessed: 15-Aug-2019].

[58] IST, "HYT 221 Module," 2017. [Online]. Available: https://www.ist-ag.com/sites/default/files/DHHYT221_E.pdf. [Accessed: 10-May-2018].

[59] A. Nicolai, J. Grunewald, and J. J. Zhang, "Recent improvements in HAM simulation tools : Delphin 5 / CHAMPS-BES," in *Proceedings of 12th Symposium of Building Physics, Marhc 29-31*

865 *2007, Dresden, Germany*, 2007, pp. 866–876.

866 [60] TBST, “Danish Building Regulations 2018,” 2018. [Online]. Available:
867 http://bygningsreglementet.dk/.

868 [61] M. Reeslev and M. Miller, “The MycoMeter-test. A new rapid method for detection and
869 quantification of mold in buildings,” *Proc. Heal. Build.*, vol. 1, pp. 589–590, 2000.

870 [62] R. A. Samson, J. Houbraken, U. Thrane, J. C. Frisvad, and B. Andersen, *Food and Indoor Fungi 1.*
871 *ed.* CBS-KNAW Fungal Biodiversity Centre, 2010.

872 [63] Mycometer, “ONSITE QUANTIFICATION OF MOULD ON SURFACES IN LESS THAN AN HOUR,”
873 2018. [Online]. Available: https://www.mycometer.com/products/mycometer-surface/about-
874 mycometer-surface/. [Accessed: 16-Nov-2018].

875 [64] Mycometer, “SURFACE SAMPLING,” 2018. [Online]. Available:
876 https://www.mycometer.com/products/mycometer-surface/surface-sampling/. [Accessed:
877 16-Nov-2018].

878 [65] Mycometer, “Mycometer ® -surface Bulk Hurtigprotokol (Danish).” pp. 1–2, 2017.

879 [66] Mycometer, “BULK SAMPLING (porous materials),” 2018. [Online]. Available:
880 https://www.mycometer.com/products/mycometer-surface/bulk-sampling-porous-
881 materials/. [Accessed: 21-Nov-2018].

882 [67] Mycometer, “Analyse af Materialeprøver med Mycometer® -Testen (Danish).” Hørsholm,
883 Denmark, 2010.

884 [68] M. Schrock, C. Riffle, A. Dindal, J. Mckernan, and J. Enriquez, “Environmental Technology
885 Verification Report: Mycometer ®-test Rapid Fungi Detection and Bactiquant ®-test Rapid
886 Bacteria Detection Technologies,” 2011.

887 [69] T. Ojanen, H. Viitanen, R. Peuhkuri, K. Lähdesmäki, J. Vinha, and K. Salminen, “Mold Growth
888 Modeling of Building Structures Using Sensitivity Classes of Materials,” in *Proceedings of*

Thermal Performance of the Exterior Envelopes of Whole Buildings XI International Conference, clearwater, Florida, USA, 2010.

[70] S. Thelandersson and T. Isaksson, "Mould resistance design (MRD) model for evaluation of risk for microbial growth under varying climate conditions," *Build. Environ.*, vol. 65, pp. 18–25, 2013.

[71] P. Johansson, "Determination of the Critical Moisture Level for Mould Growth on Building Materials," Lund University, 2014.

[72] Fraunhofer IBP, "Moisture Resistance Design (MRD) model," 2016. [Online]. Available: https://wufi.de/de/wp-content/uploads/sites/9/2016/04/Lund-MRD-model.pdf. [Accessed: 12-Jul-2019].

[73] P. Johansson *et al.*, "Threshold values for failure, linked to types of building structures and failure modes," 2019.

[74] S. Thelandersson, T. Isaksson, and J. Niklewski, "Fuktsäker utformning av klimatskiljande byggnadsdelar med fuktkänsliga material Vägledning för projektering och riskvärdering (Swedish)," Lund, Sweden, 2014.

[75] Fraunhofer IBP, "WUFI Bio," 2017. [Online]. Available: https://wufi.de/en/2017/03/31/wufi-bio/. [Accessed: 12-Jul-2019].

[76] K. Sedlbauer, "Prediction of Mould Growth by Hygrothermal Calculation," *J. Therm. ENV. BLDG. SCI.*, vol. 25, no. 4, pp. 321–336, 2002.

[77] M. Krus, M. Seidler, and K. Sedlbauer, "Comparative Evaluation of the Predictions of Two Established Mold Growth Models," in *Proceedings of Thermal Performance of the Exterior Envelopes of Whole Buildings XI*, 2010.

[78] H. Viitanen, M. Krus, T. Ojanen, V. Eitner, and D. Zirkelbach, "Mold risk classification based on comparative evaluation of two established growth models," *Energy Procedia*, vol. 78, pp. 1425–

913 1430, 2015.

914 [79] HACH, “Sension+ MM 374 GLP 2 channel Laboratory Meter for pH, ORP, ISE and Conductivity,”
915 2019. [Online]. Available: https://www.hach.com/sension-mm-374-glp-2-channel-laboratory-
916 meter-for-ph-orp-ise-and-conductivity/product?id=7640520232. [Accessed: 16-Jan-2019].

917 [80] N. F. Jensen, T. R. Odgaard, B. Andersen, C. Rode, E. B. Møller, and S. P. Bjarløv, “Supplementary
918 data for ‘Hygrothermal assessment of diffusion open insulation systems for interior retrofitting
919 of solid masonry walls.’” Technical University of Denmark, Kgs. Lyngby, Denmark, 2020.

920 [81] B. Andersen, J. C. Frisvad, I. Søndergaard, I. S. Rasmussen, and L. S. Larsen, “Associations
921 between fungal species and water-damaged building materials,” *Appl. Environ. Microbiol.*, vol.
922 77, no. 12, pp. 4180–4188, 2011.

923 [82] M. Nunez and H. Hammer, “Microbial specialists in below-grade foundation walls in
924 Scandinavia,” *Indoor Air*, vol. 24, pp. 543–551, 2014.

925 [83] V. B. Ponizovskaya, N. L. Rebrikova, A. V Kachalkin, A. B. Antropova, E. N. Bilanenko, and V. L.
926 Mokeeva, “Micromycetes as colonizers of mineral building materials in historic monuments
927 and museums,” *Fungal Biol.*, vol. 123, no. 4, pp. 290–306, 2019.

928 [84] K. Gradeci, N. Labonnote, B. Time, and J. Köhler, “Mould growth criteria and design avoidance
929 approaches in wood-based materials – A systematic review,” *Constr. Build. Mater.*, vol. 150,
930 pp. 77–88, 2017.

931 [85] E. Vereecken, K. Vanoirbeek, and S. Roels, “A preliminary evaluation of mould prediction
932 models based on laboratory experiments,” in *Energy Procedia*, 2015, vol. 78, pp. 1407–1412.

933 [86] E. Vereecken and K. Vanoirbeek, “Towards a more thoughtful use of mould prediction models :
934 A critical view on experimental mould growth research,” *J. Build. Phys.*, vol. 39, no. 2, pp. 102–
935 123, 2015.

936 [87] T. Isaksson, S. Thelandersson, A. Ekstrand-Tobin, and P. Johansson, “Critical conditions for

onset of mould growth under varying climate conditions," *Build. Environ.*, vol. 45, no. 7, pp. 1712–1721, 2010.

[88] K. Gradeci, N. Labonnote, J. Köhler, and B. Time, "Mould Models Applicable to Wood-Based Materials-A Generic Framework," *Energy Procedia*, vol. 132, pp. 177–182, 2017.

[89] E. B. Møller, B. Andersen, C. Rode, and R. Peuhkuri, "Conditions for mould growth on typical interior surfaces," in *Energy Procedia*, 2017, vol. 132, pp. 171–176.

[90] T. Ojanen, H. Viitanen, and R. Peuhkuri, "Modelling of Mould Growth in Building Envelopes - Existing Models, Discussion On Improvement Aspects." 2007.

[91] K. Gradeci, N. Labonnote, B. Time, and J. Köhler, "A probabilistic-based approach for predicting mould growth in timber building envelopes: Comparison of three mould models," in *Energy Procedia*, 2017, vol. 132, pp. 393–398.

[92] DS/EN ISO 13788, "Hygrothermal performance of building components and building elements. Internal surface temperature to avoid critical surface humidity and interstitial condensation. Calculation methods, 2. edition." Dansk Standard/Danish Standards, Charlottenlund, Denmark, 2013.